Joint Centre for Mesoscale Meteorology, Reading, UK

Analysis of an ex-tropical cyclone after reintensifying as a warm-core extratropical cyclone

K. A. Browning
G. Vaughan
P. Panagi

Internal Report No. 80

November 1997

Met Office Joint Centre for Mesoscale Meteorology Department of Meteorology
University of Reading PO Box 243 Reading RG6 6BB United Kingdom
Tel: +44 (0)118 931 8425 Fax: +44 (0)118 931 8791
www.metoffice.com

Designed and produced by the Met Office © Crown copyright 2001 01/0240 The Met Office logo is a registered trademark.

Version dated Nov 97

Analysis of an ex-tropical cyclone after reintensifying as a warm-core extratropical cyclone

K.A. Browning[1]*, G. Vaughan[2], and P. Panagi[1],

[1]University of Reading

[2]University of Wales, Aberystwyth, UK,

Summary

Ex-hurricane Lili reintensified as an extratropical cyclone before travelling across the data-rich region of the British Isles on 28 Oct 1996. The cyclone centre passed close to an MST radar providing continuous profiles of wind etc which were used to evaluate diagnostics from the mesoscale version of the operational Met Office Unified Model. The paper presents a mesoanalysis of the mature extratropical cyclone using model output together with radar and satellite observations. The combined analysis reveals a vertically extensive warm-core three-quarters surrounded by a low-level jet reaching over 40 ms^{-1}. There was an associated eye, relatively free of cloud and partly surrounded by a hook cloud producing extensive heavy rain, which was itself encircled by cooler dry-intrusion air. The stratospheric part of the dry intrusion (and its potential-vorticity anomaly) descended generally below 400 hPa, with small pockets penetrating significantly lower, within a tropopause fold around a cloud head at the leading edge of the hook cloud. The cyclone's reintensification as an extra-tropical cyclone and the development of the cloud head were closely related to its interaction with the stratospheric PV anomaly. This interaction began after the decay of the strong moist ascent and deep diabatic PV anomaly that had characterised the earlier tropical cyclone phase. The tropospheric part of the dry intrusion entered the eye region of the extratropical cyclone over a deep layer and may have been responsible for the decay of the cyclone after its rather short

* Corresponding author: Joint Centre for Mesoscale Meteorology, Department of Meteorology, University of Reading, P.O. Box 243, Reading, RG6 2BB, UK. (The Joint Centre for Mesoscale Meteorology is supported by the Meteorological Office and the Department of Meteorology, University of Reading. The collaborative research has been undertaken under theauspicies of the Universities Weather Research Network funded by the Natural Environment Research Council).

reintensification phase. The mesoscale model represented many aspects of the cyclone structure well but it underestimated the true dryness of the dry-intrusion air entering the eye. The MST radar vividly showed the region of boundary-layer air, which was responsible for the cloud head, rising up into the region of the lowered tropopause.

1. Introduction

Shapiro and Keyser (1990) describe the process by which many marine extratropical frontal cyclones evolve toward a warm-core structure during their mature stage. They present a conceptual model consistent with the results from idealised numerical simulations (eg Hoskins and West 1979, Schär 1989) and with various numerical prediction modelling and observational studies. The seclusion of warm-core air characterising the cyclone's mature stage occurs within the baroclinicity of the polar air as a result of cold polar air cyclonically encircling the low centre. Neiman and Shapiro (1993) and Neiman et al (1993) present a detailed observational case study that illustrates this process occurring over the fairly warm waters of the Atlantic off the east coast of the USA. Rapid pressure falls, well over 2 hPa h^{-1} in the Neiman study and often exceeding 1 hPa h^{-1}, can be sustained for over 24 hours during the cyclone evolution. Sometimes the rate of pressure fall diminishes as the seclusion stage is reached but on some other occasions, during this stage, there is a further period of regeneration which Grønås (1995) refers to as seclusion intensification.

Grønås identifies two kinds of regeneration : a thermodynamic intensification with similarities to the development of tropical cyclones, and intensification of what he calls the non-frontal trough, or bent-back occlusion, of strong cyclones. As an illustration of the latter kind, Grønås (1995) carried out a case study of an intense cyclone in the North Sea which deepened a

further 30 hPa during the seclusion stage. He identified the development of a low-level jet with winds of up to 60 ms^{-1} at 850 hPa on the southern flank of the warm core, the diameter of which increased from 150 to 500 km. The cyclone at this stage was characterised by distinct potential vorticity (PV) anomalies (maxima) at both lower and upper levels. The low-level anomaly was due to latent-heat release associated with abundant heavy rain (~ 4 mm h^{-1}) in the ascending parts of the moist warm-core air. The upper-level PV anomaly was associated with stratospheric air which descended to 600 hPa in the form of a streamer above the warm core. Grønås (1995) attributed the main cyclogenesis to a baroclinic development dominated by the mutual interaction of the upper-level PV anomaly and the surface temperature anomaly (Hoskins et al 1985). The latent-heat release facilitates this interaction by reducing the static stability and hence increasing the Rossby height.

Grønås also studied a case illustrating a regeneration of the first kind, in which the upper-level PV anomaly was believed not to play a significant role in the seclusion intensification process (Grønås et al 1994). In that case the cyclogenesis was attributed to the mutual interaction between the surface temperature anomaly and the low-level PV anomaly created by latent heating.

In the present paper we describe an observational and mesoscale modelling case study of a warm-core cyclone that crossed the British Isles with a structure broadly resembling the final mature stage in Shapiro and Keysers' life-cycle model and which underwent seclusion intensification as discussed by Grønås (1995). However, the cyclone in the present case was different insofar as its warm core had been in existence for many days prior to the period of reintensification. It had begun as Tropical Cyclone Lili more than a week earlier. By the time it was approaching Britain the temperature of its warm core was decreasing rapidly but its relative warmth in relation to the surrounding air was being sustained by an on-going seclusion-maintenance

process. The period of our mesoscale study (12 - 17 UTC, 28 Oct 1996) occurred shortly after an 18-hour period of deepening when there was coupling between Lili's warm core and a PV anomaly at tropopause level.

The model results used in this study are from the operational runs of the UK Met Office Unified Model (Cullen 1993). The version of the Unified Model used in 1996 was a hydrostatic, gridpoint model using spherical polar coordinates. It was run operationally in global and two different limited-area configurations. In Sec.2 we shall use output from the Limited-Area Model (LAM) version (.0.442° x 0.442°, 19 levels, 229 x 132 points, rotated pole at 30°N, 160°E) to provide an outline of the cyclone's early history over the North Atalntic. This serves as a context for the more detailed study in Sec. 4, which uses the mesoscale version of the same model (0.15° x 0.15°, 31 levels, 92 x 92 points, rotated pole at 37.5°N, 177.5°E), nested within the LAM, to diagnose the cyclone structure when it reached the British Isles. The variables required for deriving various diagnostics are held on model levels within a hybrid sigma - pressure coordinate system (Simmons and Burridge 1981) and have been re-mapped onto regular 100-hPa or 50-hPa pressure surfaces for the LAM and mesoscale versions, respectively. The mesoscale model analyses are presented in Sec. 4 but, before that (in Sec. 3), we present an observational validation of the mesoscale model. The study benefits from the good performance of the mesoscale model as the cyclone, in its mature extratropical stage, was passing over the data-rich area of the British Isles. The cyclone centre passed close to a wind-profiler radar,the Aberystwyth Mesosphere-Stratosphere-Troposphere (MST) radar, which obtained continuous soundings of wind and other properties: this was the primary source of validation data.

The mesoscale analysis in Sec. 4 addresses the 3-dimensional kinematic and thermodynamic structure of the cyclone in relation to the patterns of cloud and rain observed by Meteosat and the radar network. Characteristic features were a well-defined eye and an encircling hook cloud, both of which developed within a few hours. As in Grønås' (1995) study, the

cyclone produced an intense low-level jet. This gave surface gusts in excess of 35 m s^{-1} and caused damage in many parts of South Wales and southern England. There was also heavy rain associated with the hook cloud, and an accompanying hook-shaped region of diabatically-generated PV.

Matano and Sekioka (1971) and Brand and Guard (1978), in studying the transition of tropical cyclones to extratropical storms in the western North Pacific, have stressed the importance of intrusions of cold dry air. A dry intrusion, spiralling around the warm moist core, is a notable feature of the present case. The upper part of the dry intrusion corresponded to a streamer of descended stratospheric air, with high PV, but except for a few patches this did not descend far below 400 hPa. Beneath it, in the lower part of the dry intrusion, there was a flow of upper tropospheric origin which brought air of relatively low wet-bulb potential temperature (θ_w) into the cyclone eye from the north after spiralling around the front of the storm. A conceptual model synthesizing the overall mesoscale structure is presented in Sec. 5.

It has long been known that an upper-level disturbance can play a key role in the conversion of a tropical cyclone into an intense extratropical cyclone (Hughes et al 1955, Palmén 1956). However, the number of studies of such cyclones that have been undertaken since then is quite limited, and mesoscale studies of such situations are even fewer. Yet such events are not uncommon. About 40% of Atlantic and Pacific tropical storms progress to a stage where they interact with and transform into extratropical systems (Di Mego and Bosart 1982 a,b). Although they usually weaken after the transition as the drier air intrudes into their inner circulation, strong winds and heavy rain can continue for some time and occasionally they intensify for a period of up to 12 hours before decaying (Brand and Guard 1978). This, together with the fact that current operational NWP models do not always handle such systems well (Sinclair 1993), makes this a subject of interest to both research and forecasting communities.

2. Synoptic-scale context for the study

Surface analyses from the National Meteorological Centre (formerly the Central Forecasting Office) of the Met Office show cyclone Lili as the second of a pair of cyclones over the north Atlantic at 12 UTC on 26 October (Fig1(a)). Both cyclones travelled towards the British Isles and, by 12 UTC, 28 October, Lili was centred over Ireland (Fig. 1(c)). At this time it can be seen to have been situated well within the cold airmass and to have a bent-back front (drawn traditionally as an occlusion in this figure) extending from the main polar front far away over the North Sea.

Cyclone Lili had been travelling across the Atlantic throughout a much longer period than is shown in Fig.1. Figure 2 shows that it travelled often slowly and erratically at first while it was over the warm waters of the western North Atlantic, but then it travelled quite rapidly after 26 Oct as it came over an increasingly cool sea surface. The model output in Fig. 3(a) shows that, during the 6-day period to 12 UTC, 27 Oct, the central msl pressure fluctuated mainly within $\pm$ 3 hPa of 979 hPa (disregarding the apparent rogue model-run at 12 UTC, 26 Oct). The cyclone then deepened rapidly despite the lower sea surface temperatures, to reach a minimum of about 970 hPa at 06 UTC, 28 Oct, just before the period of our detailed mesoscale study. Figure 3(b) shows the temporal variation of the 900-hPa θ_w at the cyclone centre and of the minimum θ_w-value that completely encircled the warm core. Both were sustained at fairly high levels until 26 Oct when they began falling rapidly as the cyclone encountered significantly lower sea-surface temperatures. The difference between these two θ_w-values is a measure of the strength of the warm core; this weakened after 26 Oct but the warm core was by no means lost altogether. Figure 4, depicting the distribution of 900-hPa θ_w on 26, 27 and 28 Oct., shows the warm core continuing to exist after 26 Oct. The scale of the warm core in Fig.4(c), and its relation to a river of warm-conveyor-belt air (ie, high-θ_w air) to its southeast, resembles that in many of the extratropical seclusions analysed by Shapiro, Grønås and their co-workers as referenced in the Introduction.

The time-height plot of θ_w at the cyclone centre in Fig 3.(c) shows that until 27 Oct there was a deep layer of rather uniform θ_w with some potential instability especially during the early period. After 27 Oct the lapse rate became increasingly stable. The model's maximum convective precipitation intensity (not shown) decreased correspondingly, from 4 to 8 mm h^{-1} before 12 UTC, 26 Oct to 1mm h^{-1} or less after 12 UTC, 28 Oct. The model's dynamic precipitation intensity due to resolved ascent varied wildly between 2 and 18 mm h^{-1} before 28 Oct, and then decreased to consistently less than 2 mm h^{-1} after 29 Oct. On 28 Oct, the day of our detailed mesoanalysis, the model showed a maximum total rainfall intensity of 4 to 6 mm h^{-1}.

From a PV perspective, the sequence of events that led to the rapid redevelopment after12 UTC, 27Oct, and to the cyclone structure analysed in Sec.4, is summarised in Fig.3(d). Figure 3(d) which depicts the evolution of the vertical PV-profile at the cyclone centre, shows that, until 0UTC, 27 Oct, cyclone Lili was dominated by a strong tropospheric (diabatic) PV anomaly from 800 to 400 hPa attributable to latent heating. Probably the PV was even stronger than this since models generally underestimate the peak PV within tropical cyclones. After 0 UTC, 27 Oct the PV between 800 and 400 hPa then decreased from 4 to 2.5 PV units within 12 hours. However, following the rapid decay in the diabatic PV-maximum, there was significant descent of an upper-level PV anomaly of stratospheric origin. During the 18-hour period ending at 12UTC, 28 Oct, this was accompanied by a redevelopment in the diabatic PV anomaly due to renewed latent heat release. This led to PV values of a little over 2.5 units occurring in the lower troposphere (dashed contour in Fig.3(d)) which are more typical of intense extra-tropical cyclones than the values of 4 PV units that had previously extended up into the middle troposphere.

This interaction of the cyclone with the upper-level PV during the re-intensification is further borne out by the sequence of plan diagrams in Fig.5 which shows PV at 300 hPa (shaded areas represent high PV) and at 800 hPa (line contour represents 2 PVU). The 800-hPa PV feature is a proxy for

the cyclone's warm core: for most of the time this was the only region in the north Atlantic with PV >2 at 800 hPa. At 0 UTC, 26 Oct, Fig.5(a) shows two distinct areas of upper-level high PV, both of them rather over 1000 km away from the cyclone : one is associated with an upper trough to the north of the cyclone and the other with an upper trough to the west of the cyclone. Both converged with the position of the cyclone as time progressed, but the area of high PV that was first to interact with the cyclone was the one to the west, specifically the part marked X in Figs. 5(a to d). The feature X was a local maximum of PV which eventually broke away from the main reservoir of high PV associated with the western trough. Tracked on the 325K θ-surface (not shown) the feature X, with a maximum PV-value of 3.5 units, remained at 295 hPa from 0 UTC, 26 Oct to 12 UTC, 27 Oct as it approached the cyclone. By 12 UTC, 27 Oct, when the cyclone was starting to re-intensify, Fig. 5(d) shows that the leading edge of X was beginning to interact with the cyclone. The interaction continued to strengthen over the next 24 hours (Figs. 5(e and f)). As described in Sec. 4, this interaction was accompanied by a pronounced intrusion of dry air which circulated around the cyclone and entered its eye during 28 Oct. The source of this dry air was in the trough to the north of the cyclone rather than that to the west. Apparently the PV feature X coming from the west interacted with the upper trough to the north as it approached the cyclone. It would seem that both troughs had some influence on the re-intensification of the cyclone.

The 48-hour forecast valid at 12 UTC on 28 Oct showed a substantial error in the prediction of the cyclone for both the Unified Model and the ECMWF model. For the latter, the analysed surface pressure minimum was 970 hPa whereas the forecast gave 992 hPa. Using the method of localised singular-vector computation with the ECMWF model, as described in Buizza and Montani (1997), it is possible to find the location of the region, 48 hours before the time of the erroneous forecast, in which any analysis error would have grown rapidly to reduce the skill of the forecast of the low in question over the British Isles. To make this computation Montani and Thorpe (private communication) defined an area (10°W to 5°E and 45°N to 60°N) containing

the low at 12 UTC on 28 Oct (the "final time"). The singular vectors (SVs) were then computed at 12 UTC on 26 Oct (the "initial time"). The region with the largest amplitude was found to be located at an altitude of 7km near and somewhat upstream of the PV anomaly labelled X.

The way in which the interaction with the upper-level PV affected the cyclone structure is described in the following sections. To study the 3-dimensional structure of the cyclone in detail it is necessary to use mesoscale model output. But before doing this we make use of the special observations from the Aberystwyth MST radar to reveal certain shortcomings of the model performance at the same time as providing confidence in its overall ability to represent the 3-dimensional structure.

3. Evaluation of the performance of the mesoscale model using MST radar profiles.

The ability of the Unified Model to produce satisfactory analyses and forecasts at mesoscale resolution using operationally available sources of data has been demonstrated by Ballard et al (1993). In the present study, however, we shall be very demanding in our use of the model, by employing it to diagnose the vertical structure of the cyclone in considerable detail. For this reason we shall exploit a particularly useful time series of profiles provided by the MST radar as cyclone Lili travelled over Aberystwyth. We confine the evaluation to the layer between 1.7 and 14 km (the design of the radar presents measurements from being obtained at lower levels). To some extent the evaluation is compromised by the fact that 3-hourly MST wind profiles are already assimilated into the operational Unified Model suite. In reality, however, these profiles receive an uncertain and sometimes relatively small weight in relation to the background field obtained from earlier forecast runs of the model and so there is no guarantee that the model will faithfully reproduce all the observed structures. In any case, the MST profiles used in this study were obtained virtually continuously and this makes it possible to validate small-scale features that the model may generate in the absence of

observational inputs on such scales. Additional evidence for the realism of the model will be given in Sec.4 where the model output is presented alongside observational data such as the rainfall and cloud fields from radar network and satellite imagery.

(a) The MST radar time-height sections

The UK MST radar at Aberystwyth (52.4°N, 4.1°W), sited at an altitude of 90m, operates at 46.5 MHz, with peak power 160 kW and antenna area $10^4 m^2$. A full description may be found in Slater et al (1991). For this work, a pulse length of 8μs was used, phase-coded with 2μs segments corresponding to a range resolution of 300m. The beam was successively steered to the vertical, SE6, SE12, NE6, NW6 and NW12 directions (SE6 means 6° zenith angle towards the south-east) with dwell times of 20s: spectra for a particular direction were averaged over 12 minutes before processing. Details of the setup of the radar for this day may be found in Worthington and Thomas (1996).

The primary products of the radar used in this paper are time-height patterns of the vertical echo power and the three wind components derived from the SE6, NE6 and vertical beams. The radar-derived u-and-v-components of the wind are shown in colour in Figs. 6(a) and 6(b), respectively. These wind fields are discussed shortly in Sec.3(b). Winds are measured with these 3 beams from 1.7 to 14km with precision $1.2 ms^{-1}$ (standard deviation) for 12-minute average spectra (Astin and Thomas 1992). The horizontal wind components derived this way are systematically lower by 4-6% than those measured by radiosondes because of the aspect sensitivity of VHF radar echoes and the finite width of the radar beam (Thomas et al 1997). This can be corrected using echoes at 4.2° and 8.5° zenith angle, but these directions were not used on 28 October 1996. Winds derived from the vertical and 12° beams are more accurate but the lower echo power leads to poorer precision and gaps in the measurements.

The time-height pattern of radar echo power is shown in Fig.7. A number of salient features may be derived from the vertical echo power measurements. The power in this direction is generally proportional to M^2, where M is the mean vertical gradient in potential refractive index (Ottersten 1969). In the upper troposphere and stratosphere M is closely related to the static stability and so the radar may be used to identify the tropopause (Vaughan et al 1995), which normally corresponds to the maximum (positive) power gradient beneath the secondary maximum in power in the 8-14km region. Such a gradient may be seen descending from 11km at 0 UTC to 9.5km at 0830 UTC and at around 10 km from 18 to 24 UTC. In between, the high power (>50dB) in the upper troposphere indicates an indefinite tropopause, with a gradual transition from tropospheric to stratospheric stability (Fig.8), as encountered in tropopause-fold regions and where the upper-level flow is cyclonic. We elaborate on this later.

In the lower part of the troposphere, humidity gradients also contribute to M. In an unsaturated atmosphere an acceptable model for the power may be constructed by assuming that small-scale vertical displacements of air conserve potential temperature and specific humidity (Ottersten 1969, Luce et al 1995). The radar data in Fig.7 show, from 4UTC to 11UTC, a layer of low power near 4km, corresponding to the very dry layer found in a nearby Aberporth radiosonde profile at 5UTC (not shown). Beneath this there was a moist layer with high echo power corresponding (on this day) to the planetary boundary layer. The well defined power maximum at 2.5km between 4 and 10 UTC corresponds to the top of the boundary layer where the humidity gradients were greatest. (The MST radar-derived depth of the boundary layer is in agreement with the height (temperature) of the boundary-layer cloud identified in the Meteosat infrared imagery). A similar power maximum can be seen just above 4km at the end of the day, for the same reason. At about 10UTC the power maximum representing the top of the moist layer begins to ascend. Then, after 14 UTC the level of the power maximum, corresponding to the top of lifted boundary-layer air rather than the top of the boundary layer per se, rises markedly before falling again at 17 UTC and during this period

it merges in the power profile with the signature of the descended tropopause. The general weakening in the radar power during this time is associated with a period of heavy rain, a commonly observed association which is not well understood.

(b) Comparisons of the Unified Model time-height sections with those from the MST radar.

Vertical wind profiles for the Aberystwyth location have been extracted from the mesoscale model for 4 consecutive 6-hour periods corresponding to forecast runs starting at 0,6,12 and 18 UTC, 28 Oct. For comparison with the height profiles provided by the radar it is necessary to remap the model data onto surfaces of fixed height (metres). We have used surfaces at 500m intervals, up to a height of 14km, and linearly interpolated the various diagnostics where necessary. The Unified Model grid point nearest to the radar, at which the time-height cross-sections were taken, has a latitude and longitude of (52.34°N,4.22°W) and is at sea level. The model-derived u-and v-wind components are superimposed on the observations from the MST radar in Figs.6(a) and 6(b).

The overall agreement between model and radar is good. The patterns are qualitatively similar and difference fields (not shown) demonstrate agreement generally to within ± 5 m s^{-1}. The most significant discrepancies are in the v- component; in particular, the model underestimates by typically 5 to 8 m s^{-1} the large southerly wind components occurring in the height range 4 to 8km for an hour or so centred at 11 UTC and then again it underestimates (by 5 to 10 m s^{-1}) the large northerly components occurring in the height range 4 to 8km for a period of up to 2 hours centred at 20 UTC. The generally good agreement encourages us to use the model output in some detail in Sec. 4, especially when drawing qualitative conclusions: however, it is necessary to keep in mind the above limitations especially the underestimation of the northerly winds between 4 and 8km altitude just after the passage of the cyclone centre. A significant feature, only partially

observed by the radar because of its minimum-range limitations, is the low-level jet at 15 UTC. Both radar and model see this jet as a localised maximum, with the u-component reaching 28 to 30 m s^{-1} and the v-component reaching 25 m s^{-1} albeit with a small discrepancy in timing.

The wind profiles constitute the most direct evaluation data provided by the MST radar. However, the other form of radar measurement which, although only an indirect evaluation of the model is nevertheless also useful, is the intensity of the radar echo expressed in terms of the logarithm of the received power (Fig.7). As explained above, the radar echo pattern enables us to identify two key features. One of these is the tropopause which can be compared with the model's PV-distribution. The other is the top of the boundary-layer air which can be compared with that evident from the model-derived moist layer. The MST radar also provides a direct measure of vertical velocity but, although this does reveal the main region of ascent predicted by the model, we choose not to show it because in the hilly Aberystwyth region this was often contaminated by gravity waves.

To facilitate the comparisons of tropopause and boundary-layer depth, a digest of the model results is superimposed on the radar results in Fig.7. The upper white line is the model's tropopause: this has been taken as PV=3 to avoid any possibility of contamination with the diabatically generated tropospheric PV (a more realistic height for the tropopause (PV=2) would be about 500m lower). Note the good agreement with the base of the radar power maximum (green layer in Fig 7) associated with the tropopause. Between 8UTC and 16UTC where the radar indicates an indistinct tropopause, there is nevertheless an indication of multiple radar echo layers continuing to descend in line with the model-derived tropopause.

Another useful piece of observational evidence, close to the cyclone centre, is provided by the ~~nominal~~ 18 UTC radiosounding made at Aberporth, 40 km southwest of Aberystwyth. Figure 8 shows the 18 UTC model-derived sounding superimposed upon the Aberporth sounding. Neglecting features

with vertical scale 50 hPa or less, the general fit of the temperature curve is good and perceptably better than that for model-derived soundings extracted 2 hours before or after (not shown). However, the dew-point curve does not fit as well, partly because of the excessive smoothing in the model as a result of which the drying out at the top of the boundary layer is underestimated and occurs over a depth of 1 km rather than abruptly. The precise estimate of the boundary-layer top from the model is thus rather arbitrary. The lower white line, labelled 80, in Fig 7 shows the model's 80% relative humidity. This fits the radar-derived top of the moist layer (i.e. the radar power maximum) quite well, including the way in which the top of the moist layer rises steeply to a maximum between 14 and 18 UTC. This vertical extension of moist air occurred during the passage of the cloud-head feature discussed in Sec 4(a). As noted earlier, the radar power decreased in this rainy cloud-head region but a weak maximum in power can nevertheless be seen rising to at least 6.5 km on either side of this region, and there is a hint of a maximum in power, suggestive of an upper limit to the moist air, at 8 km at 16 UTC. The model, on the other hand, has moist air rising here to 9km. The model even has moist air penetrating into its own region of stratospheric air which one would normally expect to be dry. This is perhaps due to excessive vertical diffusion in the model.

4. Mesoscale analysis of cyclone Lili following reintensification as an extra-tropical cyclone.

(a) Formation of the cloud head (09-17UTC)

Cyclone Lili developed a striking structure immediately after it attained its minimum msl pressure as it crossed Ireland. This was evident in satellite imagery (Fig. 9) through the formation of a hook-shaped cloud and an eye during the period from 9 to 17 UTC, 28 Oct. (The time sequence in this and later figures ends at 17 rather than 18 UTC as might seem more logical; we avoid the later time because by then the system was beginning to show signs of decay and loss of organization). The eye is not an eye in the full sense

normally applied to a tropical cyclone but simply a region containing very little cloud The imagery makes the eye appear almost cloud-free at times but generally the eye was filled with low stratus. Observations from weather radar (Fig.10) indicate that the eye was mainly dry and the hook cloud itself was associated with an extensive area of continuous rain which increased in intensity from moderate to heavy between 12 and 15 UTC. The heaviest rain was in the cloud-head region (ie the leading part of the hook cloud) located over the Irish Sea in Fig.9(c). Adjacent to the cloud-head, over northern and western England, the radar shows extensive showers. According to the satellite infrared imagery these were due to shallow convection within a boundary layer, the top of which increased towards the cyclone as shown in Fig.7.

During the period, 12 - 17 UTC, the mesoscale model showed a rolling up of PV features which paralleled the development of the hook and eye. This was evident both in the low troposphere (Fig.11(a)) where the high PV was due to latent-heat release in the hook cloud, and at upper levels(Fig. 11(b)) where the high PV was due to the involvement of stratospheric air into the cyclone circulation. The latter corresponds to the tropopause depression that was seen in Fig.5 converging with the cyclone during the previous two days. Unlike the mesoscale model, the Limited-Area model results in Fig. 5 did not resolve the roll-up process on the scale of the hook and eye.

Figure 11(c) shows the satellite-detected extent of cloud colder than -25°C, corresponding approximately to the 400-hPa level. This is to be compared with Fig.11(b) which shows a tongue of low-PV tropospheric air (unshaded) interlaced within the spiralling region of stratospheric air at 400 hPa. This unshaded region corresponds to air that had risen in the leading (cloud-head) portion of the hook cloud into the region of the tropopause depression. The rate of development of this feature in the model (Fig. 11 (b)) relates well to the rate of advance of the cloud head as observed by the satellite (Fig. 11(c)).

b) The 3-dimensional thermodynamic structure at 15UTC

The period of maximum rainfall intensity for the extra-tropical phase was 15 to 17 UTC, 28 Oct. This was also the period when the cloud head and eye were best developed. After 15 UTC the structure became increasingly complicated by the effects of orography over England and Wales and so we shall concentrate in this section on the time 15 UTC. The 3-D thermodynamic structure at this time is depicted in the plan sections in Fig.12. Figure 12(a), giving the potential temperature at upper, middle and lower levels, shows that the warm-core structure extended as an upright column throughout the troposphere. The strongest winds associated with the cyclone were within a low-level jet at 900 hPa (Fig.12(b)). Speeds in excess of 30 ms^{-1} can be seen around three-quarters of the perimeter of the warm core, with peak values of over 42 ms^{-1} on the south side where the cyclone's motion added to the system-relative circulation. This is the part of the storm that later caused damage in parts of southern Britain. Gusts up to 40 ms^{-1} were recorded in South Wales. At upper levels the main polar jet can be seen in Fig,12(b) to the southeast of the cyclone, extending from west of Brittany to Norway.

A further indication of the 3-dimensional structure is provided by Figs.13 (a-d), which show model-derived parameters within a vertical section along AA' in Fig.12(a). Salient features from Fig.13 are synthesised in Fig.14 to show their inter-relationships. The dry-and wet-bulb potential temperature patterns in Fig.13(a) show the warm core extending up to about 300 hPa, although the major warm anomaly occurs between the surface and 500 hPa. The position of the warm core is represented crudely in Fig.14 by the θ_w=12°C isopleth and stippled shading. Figure13(b), depicting the magnitude of the wind velocity, shows the main upper-level jet (J_u) associated with the polar front in the top right corner; it also shows 2 wind maxima (J_L) at 900 hPa, separated by 400 km, where the section intersects the low-level jet on either side of the warm core. These are represented in Fig.14 by the J_L labels and a perspective visualization of the associated circulation. The axis of minimum

windspeed is almost colocated with the axis of the warm core and is plotted in Fig.13(b) as a dashed line.

Figure 13(c) shows the distribution of PV, from which the dynamical tropopause (PV=2 units) is seen to dip down to 480 hPa (approx. 6km)at x = 900 km as part of the tropopause depression just ahead of the warm core. This is consistent with the observational evidence from the MST radar (Fig.7). At the top of the warm core, near the 400-hPa level between x = 450 and 700 km in Fig. 13 (c), there are patches of high PV which, as shown in Fig.11(b), are part of a tropopause depression (PV streamer) that has been carried around the axis of the warm core.This spiralling of the tropopause depression is represented in Fig.14 by a simplified version of Fig.13(c) that is consistent with Fig.11(b). The tropopause depression is part of a general region of lowering PV contours extending down into the middle troposphere ahead of the cyclone as shown by the dashed line SS in Fig 13(c). The overall 3-D structure of streamer SS is discussed in Sec.4(c). Within the cyclone's warm-core region, centred at x=670km, Fig.13(c) shows a column of air with PV≥ 2 units extending from 900 to 500 hPa where it merges with the high-PV streamer of stratospheric air that has been carried around and intruded toward the axis of the warm core aloft. According to Fig.13(d) all of the column, except for the streamer of stratospheric air that has intruded towards the axis of the warm core at 400 hPa, was within a region of essentially saturated air. This diabatically generated column of high PV was associated with the hook cloud's main rain area (ie the cloud head) and is represented in Fig.14 by horizontal hatching. Another, smaller, area of diabatically generated PV is associated with the band of rain on the left (north west side) of the warm core.

The pattern of relative humidity in Fig.13(d) shows a moist boundary layer capped by dry air on both sides of the cyclone. We showed in Sec.3 the tendency for the model to smooth out a sharp moisture boundary vertically over 1 km and, accordingly, we have represented the likely true cloud boundary by the model-derived RH=80% isopleth (wavy line) in Fig. 14. This

draws attention to the main region of deep cloud associated with the cloud head ahead of the eye. Between the cloud head and the other moderately deep cloud area centred at x = 350km, the unsaturated column of air corresponding to the eye extends down to 700hPa.

(c) Penetration of the dry intrusion into the eye region.

We showed in Sec. 4(a) that the formation of the hook-and-eye structure was associated with the cyclonic rolling up of the upper-level PV maximum corresponding to a tropopause depression or tropopause fold (Fig.11(b)). Viewed in vertical section the streamer-like region corresponding to the axis of the PV fold (SS in Fig.13(c)) extends down into the low troposphere and is associated with the edge of very dry air wrapping around the cyclone's warm core. The horizontal position of streamer SS at different levels is shown in Fig.15(a) encircling the column of diabatically generated PV as represented by the area of PV=1.5 units at 500 hPa. At the 300 and 400-hPa levels the axis of maximum PV is located within the stratosphere and it extends in an S-shape past the cyclone, with only part of it turning inwards toward the cyclone centre. At 500,600 and 700 hPa, the axis of maximum PV is within the troposphere and most of it turns inwards towards the cyclone's northeast quadrant. The axis of the streamer is situated farther away from the cyclone at the lower levels, consistent with the slope of SS in Fig.13(c).

The penetration of the lower part of the streamer SS into the cyclone eye is shown by the plan section at the 700-hPa level in Figs.15(b), (c) and (d) on each of which is marked a dashed line representing air approaching the eye. The PV pattern in Fig.15(b) shows that the dashed line corresponds to the PV streamer SS where it was recognizable ahead of the cyclone (diabatic processes modify the PV as the air nears the cyclone centre). The pattern of relative humidity in Fig.15(c) shows that the streamer SS is on the edge of the very dry air and that some relatively dry air penetrates along the dashed line into the cyclone eye. (The model underestimates the dryness of this air as it approaches the cyclone because of the excessive smoothing

identified in Sec.3). The pattern of θ_w in Fig.15(d) shows that the same dashed line corresponds to the axis of a flow of low-θ_w air penetrating into the eye. The flow of air along this dashed line, characterised by low θ_w, low relative humidity and initially high PV, is the dry intrusion.

A well defined, elongated 'dark zone', indicative of dry-intrusion air in the upper-and middle troposphere, was evident in the Meteosat water vapour imagery at 15 UTC (not shown). The axis of the dark zone was close to the axis of maximum PV at 600 hPa and it extended the full length of the corresponding dashed line in Fig. 15(a). The end of the dark zone nearest the cyclone centre actually extended beyond the end of the dashed line in southwest Scotland, down the east coast of Ireland, right into the cyclone centre.

We now consider the effect of the dry intrusion as it enters the eye-region of the cyclone below the level represented by the satellite dark zone. The encroachment of the dry intrusion in the lower troposphere is shown best by the distribution of θ_w. Figure 16, depicting a sequence of θ_w -patterns in the eye region at 900, 800 and 700 hPa, shows a low -θ_w notch intruding on the northern flank. It also shows a tendency for the low -θ_w notch to penetrate farther at 700 hPa than at 800 or 900 hPa, ie there is a tendency for overunning, leading to potential instability. This is the same tendency as revealed in a study by Browning et al (1997), albeit in that case for a less mature cyclone in which the overrunning occurred on the south flank of the cyclone before the dry intrusion had a chance to spiral around it.

5. Synthesis

We have described the structure and evolution of an Atlantic cyclone after it underwent a transition from a tropical cyclone (Lili) to an extratropical

cyclone. During its intense extratropical stage the cyclone retained an upright warm core up to 400 hPa. Nevertheless its structure in some ways resembled that of other extratropical cyclones that have reached a mature stage at the end of an entirely extratropical evolution. Specifically, it resembled the 'warm-core frontal seclusion' corresponding to the fourth and final stage in Shapiro and Keysers' (1990) life-cycle model. This stage, with its warm-core structure, has been evidenced by several recent case studies (eg Neiman and Shapiro (1993), Neiman et al (1993), Grønås (1995)). However, whereas in the Shapiro-Keyser life-cycle model, the warm core develops within the baroclinicity of the polar air by cold polar air encircling the cyclone centre, in the present case the same process acted not to *develop* the warm core but rather to *sustain* a pre-existing warm core against decay as it travelled over colder seas. The warm core was sustained over virtually the full depth of the troposphere.

We showed in Sec. 2 how, from before 20 Oct until 26 Oct 1996, cyclone Lili had had a diabatically generated PV maximum of 4 PV units extending above 500 hPa, a warm-core θ_w-maximum of 22 to 25°C at 900 hPa, and a 900 hPa warm-core anomaly of 3 to 4°C, (Fig.3). But then, as it travelled rapidly east-northeastwards, it lost most of its high PV in the troposphere and the θ_w-maximum plummeted, dropping 8°C in the 36 hours commencing O UTC 27 Oct. Yet, despite this, it retained a warm core (albeit with a smaller anomaly of 1 - 2°C at 900 hPa) because, after an initial lag, the region where polar air was encircling it was cooling as rapidly as the warm core itself. This was related to a period of rapid cyclogenesis associated with the interaction with an upper-level PV anomaly. Between 12 UTC, 27 Oct and 06 UTC, 28 Oct the central msl pressure dropped from 980 to 969 hPa and a positive PV anomaly redeveloped in the low troposphere with a magnitude similar to that typically encountered in intense extratropical cyclones. The mature stage of the cyclone occurred after the period of rapid deepening, notably from 09 to 17 UTC, 28 Oct, when it developed a striking structure evident in imagery as a hook and eye.

The portrayal of the three-dimensional structure of the mature extratropical cyclone in Sec 4 is, despite our best endeavours, rather complex. Yet there is an overarching simplicity in the cyclone structure. This is shown by the 3-D schematic in Fig.17 which provides a qualitative framework within which to interpret the more quantitative results given in the earlier figures.

The lower part of the cyclone, with its low-level jet, is depicted in Fig.17 as a cylinder sliced off at 700 hPa. This in turn is shown cut in half by a vertical section, orientated northwest-southeast, which shows the top of the boundary-layer air rising towards the cyclone centre. In the leading (eastern) part of the cyclone there were abundant convective showers within the boundary layer. Closer to the cyclone centre these showers gave way to deep stratiform ascent and widespread heavy rain associated with the cloud head at the leading edge of the hook of cloud that wrapped around an eye. The eye itself was devoid of cloud except at the lowest levels.

Encircling the hook cloud was a broad flow of very dry air (<10% relative humidity) which corresponds to a dry intrusion, as summarized by Browning (1997).The dry intrusion is represented by three tubular arrows in Fig.17: the top one represents dry stratospheric air with high PV above a tropopause depression, descending towards a tropopause fold at the leading edge of the hook cloud. Much (but not all) of the lower stratospheric air shown by the upper arrow continues past the cyclone via the fold region without turning in towards the eye. The other two tubular arrows represent dry near-tropopause air and tropospheric air, respectively, descending within and beneath the tropopause depression. Parts of all these flows circulated around the cloud head and then in towards the eye but, unlike in the case studied by Grønås (1995), it is probably only the tropospheric flow that penetrated to any depth in the cloud-free eye.

Experience with using both Limited-Area and Mesoscale versions of the Unified Model to trace thin filaments of stratospheric air within tropopause folds indicates that, whereas the Limited-Area Model may see such filaments as regions with PV~1, the Mesoscale model is better able to resolve them as PV=2. The present mesoscale model diagnostics suggest that most of the stratospheric air failed to get below 500 hPa. However, the model did show small pockets of very dry air with relatively high PV circulating within the streamer down to quite low levels just above the boundary layer ahead of the cyclone's cloud head. One such pocket of stratospheric air, with a PV-value in excess of 2, can be seen at 700 hPa just north of East Anglia in Fig.15(b). It may have been this or another similar pocket of stratospheric air that produced the exceptionally dry layer between 700 and 600 hPa in the 05 UTC Aberporth radiosounding (not shown). According to the MST radar, turbulence could be detected in the form of 2 m s^{-1} spectral widths from 0530 until 1000 UTC in advance of the cloud head at about 700 hPa, where the relatively high- PV air of the streamer was grazing the top of the boundary layer. Stronger turbulence (spectral width >3 m s^{-1}) was measured at high levels within and at the rear edge of the cloud head; some of this may have been associated with the stratospheric streamer where it intruded into the upper part of the cloud head.

The eye was a notable feature of the satellite imagery. It was not as compact as a tropical cyclone eye but 'eye' is nevertheless an apt description. It formed from a barely perceptible feature at 09 UTC 28 Oct to become a major feature, about 200 km across, six hours later (Fig.9(c)). It developed as a result of the hook cloud wrapping cyclonically around a relatively cloud-free region characterised by dry-intrusion air, in the same way that a 'cloud head' wraps around a 'dry slot' as described by Browning and Roberts (1994) in the case of a normal extratropical cyclone. In the present case, however, the cyclonic wrap-up proceeded so far that one needs to view the satellite images upside-down to recognise the similarity with the Browning-Roberts description. This process of hook-cloud formation began just as the upper-

level PV- anomaly was beginning to wrap around the diabatically-generated low-level PV - maximum

The relatively cloud-free nature of the eye owed its origin, as already mentioned, to the mainly tropospheric component of the dry-intrusion flow which brought relatively dry, low-θ_w air into the eye from the north after circulating cyclonically around the cloud head (see Figs.15 (c and d)). On the whole we have gone ahead rather confidently in using the mesoscale model results because of the good validation evidence in Sec.3(b). However, a significant shortcoming of the model run also pointed out in Sec. 3(b) was its failure to introduce sufficient dry northerly flow into the eye region.

The showers that preceeded the cyclone were located beneath the dry intrusion as it encircled the moist warm-core, both to the east of the cloud head, and to the north and south of it (Fig.10). Rainfall was heavy in many of these showers, especially when they came inland over the mountains. The showers were confined vertically within a boundary-layer whose depth increased as the cyclone approached. This ascent of the top of the boundary-layer air within the cloud head as the cyclone approached was strikingly shown by the MST radar, as was the lowering of the tropopause which was bringing down high PV during the same period.

6. Conclusions

On 28 Oct 1996 ex-hurricane Lili travelled across the data-rich region of the British Isles. The detailed analysis of the cyclone at this time showed a warm-core frontal seclusion, corresponding to the fourth and final, mature, stage of Shapiro and Keysers' (1990) cyclone life-cycle model. The warm core in the present case, however, reached up to above 400 hPa, which is deeper than in most extra-tropical seclusions. Its rather upright warm core had been cooling rapidly for over 2 days as a result of passing over cooler

waters but it continued to be warmer than its surroundings because cooler polar air was cyclonically encircling it.

The inner regions of the cyclone consisted of an eye with a hook of deep cloud and widespread stratiform rain that unfolded around the eye over a period of 6 hours. Around the eye there was a zone of strong winds that reached a maximum of 35 to 40 m s^{-1} at 900 hPa at a radius 200 km. Outside of this region, the boundary layer deepened as the hook and eye approached and it produced frequent shallow convective showers before the arrival of the leading part of the hook cloud, referred to as the cloud head. Above the boundary layer, dry-intrusion air circulated around the cloud head. The lower part of the dry intrusion was tropospheric air which spiralled into the eye on its northern side and may have hastened the decay of the cyclone. The upper part of the dry intrusion was stratospheric air, with high potential vorticity. Except for odd pockets of high-PV air which descended to 700 hPa, most of the stratospheric air descended only to between 400 and 500 hPa. Nevertheless, it appeared to play a major role in the reintensification process. Singular-vector analysis by Montani and Thorpe (private communication) showed that a 2-day forecast of the extratropical reintensification of Lili was particularly sensitive to the quality of the initial data upstream and just below the level of the upper-level PV anomaly that interacted with the cyclone. Additional observations targeted in such regions are probably needed if we are to improve forecasts of these potentially hazardous events.

Acknowledgements

We are grateful to the Met Office for access to the Unified Model and other data, to Ed Dicks for deriving some of the products, Gavin Winter for assistance in data processing, Alan Thorpe and Andrea Montani for supplying results of singular vector computations and Chris Thorncroft for helpful discussions

References

Astin, I and Thomas, L. 1991 The accuracy and precision of radar wind measurements, Proceedings of the fifth workshop on technical and scientific aspects of MST radar, ed. B.Edwards, SCOSTEP, U, of Illinois Urbana, USA, pp 15-20.

Ballard, S.P., Robinson, R., Barnes R.T.H., Jackson, S. and Woltering S. 1993 Development and performance of the new mesoscale model. Forecasting Research Tech. Rep. 40, 68 pp. [Available from National Meteorological Office Library, London Road, Bracknell, Berkshire RG12 2SZ, United Kingdom].

Brand, S. and Guard, C.P. 1978 Extratropical storm evolution from tropical cyclones in the western North Pacific Ocean. Tech. Report TR 78-02 Naval Environmental Prediction Research Facility, Monterey, California. July 1978, 20 pp.

Browning K.A, Balland, S.P. and Davitt, C.S.A. 1997 High-resolution analysis of frontal fracture. *Mon.Wea.Rev.*, **125**, 1212-1230.

Browning K.A. and Roberts, N.M. 1994 Structure of a frontal cyclone. *Q.J.R.Meterol. Soc.*, **120**, 1535-1557.

Browning, K.A. 1997 The dry intrusion perspective of extratropical cyclone development. *Met.Apps.*, **4**, In press.

Buizza, R and Montani,A. 1997 Targeting observations using singular vectors: methodology and preliminary results, *Q.J.R.Meteorol.Soc*, submitted.

Cullen, M.J.P., 1993 The unified forecast climate model, *Meteorol. Mag.*, **122**, 81-94.

DiMego, G.J. and Bosart, L.F. 1982a The transformation of Tropical Storm Agnes into an extratropical cyclone. Part I : The observed fields and vertical motion computations. *Mon.Wea.Rev.*, **110**, 385-411.

DiMego, G.J. and Bosart, L.F. 1982b The transformation of Tropical Storm Agnes into an extratropical cyclone. Part II : Moisture, vorticity, and kinetic energy budgets. *Mon.Wea.Rev.*, **110**, 412-433.

Grønås, S, 1995 The seclusion intensification of the New Year's day storm 1992 *Tellus* **47A**, 733-746.

Grønås, S, Kvamstø, N.G. and Raustein, E. 1994 Numerical simulation of the northern Germany storm of 27-28 August 1989. *Tellus* **46A**, 635-650.

Hoskins, B.J. and West, N.V. 1979 Baroclinic waves and frontogenesis, Part II Uniform potential vorticity jet flows - cold and warm fronts *J.Atmos.Sci.*, **36**, 1663-1680.

Hoskins, B.J., McIntyre, M.E. and Robertson, A.W. 1985 On the use and significance of isentropic potential vorticity maps. *Q.J.R.Meteorol.Soc.*, **111**, 877-946.

Hughes, L.A., Baer, F., Birchfield, G.E. and Kaylor, R.E. 1955 Hurricane Hazel and a long-wave outlook. *Bull.Amer.Meteorol.Soc.,,* **36,** 528-533.

Luce, H., Crochet, M., Dalaudier, F. and Sidi, C. 1995 Interpretation of VHF ST radar vertical echoes from in-situ temperature sheet observations. *Radio Sci.,* **30,** 1003-1025.

Matano, H . and Sekioka, M. 1971 Some aspects of extratropical transformation of a tropical cyclone. *J.Meteorol.Soc.Japan,* **49,** 736-743.

Neiman, P.J. and Shapiro, M.A. 1993 The life cycle of an extratropical marine cyclone. Part I : Frontal-cyclone evolution and thermodynamic air-sea interaction *J.Atmos.Sci.,* **121,** 2153-2176.

Neiman, P.J. and Shapiro, M.A. and Fedor, L.S. 1993 The life cycle of an extratropical marine cyclone. Part II : Mesoscale structure and diagnostics. *J.Atmos.Sci.,* **121,** 2177-2199.

Ottersten, H. 1969 Mean vertical gradient of potential refractive index in turbulent mixing and radar detection of CAT.*Radio Sci.,* **4,** 1247-1249.

Palmén, E. 1958 Vertical circulation and release of kinetic energy during the development of hurricane Hazel into an extratropical storm. *Tellus,* **10,** 1-23.

Schär, C.J. 1989 Dynamische Aspekte der aussertropischen Zyklogenese, Theorie und numerische Simulation im Limit der balancierten Strömungssysteme, Dissertation Nr. 8845 der Eidgenossischen Technischen Hochschule, Zurich, 241 pp.

Shapiro, M.A. and Keyser, D. 1990 Fronts, jet steams and the tropopause, Pp 167-191 in *Extratropical cyclones*. Eds.C.W. Newton and E.O. Holopainen, American Meteorological Society, Boston, Mass.

Simmons, A.J. and Burridge, D.M. 1981 An energy and angular momentum conserving finite difference scheme and hybrid coordinates. *Mon.Wea.Rev.*, **109**, 758-766.

Sinclair, M.R. 1993 Synoptic-scale diagnosis of the extratropical transition of a southwest Pacific tropical cyclone. *Mon.Wea.Rev.*, **121**, 941-960.

Slater,K., Stevens, A.D.,Pearmain, S.A.M., Eccles, D., Hall. A.J., Bennett. R.G.T., France,L.,Roberts, G., Olewicz, Z.K., Thomas, L., 1991 Overview of the MST radar system at Aberystwyth. Proceedings of the fifth workshop on technical and scientific aspects of MST radar, ed B. Edwards, SCOSTEP, U of Illinois, Urbana, USA, pp 479-482.

Thomas. L., Astin, I and Worthington, R., 1997 A statistical study of underestimates of wind speeds by VHF radar. *Ann Geophys.*, **15,** 805-812.

Vaughan, G., Howells, A and Price, J.D., 1995 Use of MST radar to probe the mesoscale structure of the tropopause.*Tellus*, **47A,** 759-765.

Worthington ,R.M, and Thomas, L 1996 The measurement of gravity wave momentum flux in the lower atmosphere using VHF radar. *Radio.Sci*, **31,** 1501-1517.

Figure legends

Fig.1. Surface analyses from the UK National Meteorological Centre for 12 UTC on (a) 26 Oct, (b) 27 Oct and (c) 28 Oct 1996.

Fig 2 Track of cyclone Lili, 20-29 Oct 1996, showing locations at 0 UTC on each day, superimposed on isopleths of sea surface temperature.

Fig.3. Time records from 20 to 29 Oct 1996, for cyclone Lili, as obtained from analyses of the Limited-Area version of the operational Met Office Unified Model: (a)minimum mean-sea-level pressure, (b) maximum warm-core value of 900-hPa wet-bulb potential temperature (θ_w) (crosses) and minimum value of θ_w that completely encircles the warm core (circles) (c) vertical profile of maximum θ_w within 100 km of cyclone centre, and (d) vertical profile of maximum potential vorticity within 200km of cyclone centre. The pair of vertical lines, at 12 and 17 UTC, 28 Oct, denote the period of the detailed mesoanalysis.

Fig. 4 Wet-bulb potential temperature analyses at 900 hPa (contours at 1°C intervals from 3 to 23°C, warm areas shaded more heavily) at 0 UTC on 26, 27 and 28 Oct 1996, as derived from the Limited-Area version of the operational Met Office Unified Model. L shown alongside a θ_w-maximum, marks the warm core associated with cyclone Lili.

Fig.5(a-f). Potential vorticity at 300 hPa (grey scale with shading corresponding to PV=2,4,6 and 8 PV units) and 800 hPa (single contour for 2 PV units), as derived at 12-hour intervals from 0 UTC, 26 Oct to 12 UTC, 28 Oct 1996, from analyses of the Limited-Area version of the operational Met Office Unified Model. The low-level PV-maximum (almost-circular closed contour) represents the location of the cyclone. The feature X denotes the area of upper-level PV that interacted most strongly with the cyclone.

Fig. 6. Time-height sections of (a) zonal (u) and (b) meridional (v) wind components at Aberystwyth from 0 to 24 UTC on 28 Oct 1996 as obtained from the MST radar profiler and four mesoscale-model 6-hour forecast runs starting at 0, 6,12 and 18 UTC. Colours and line contours, respectively, represent winds in m s^{-1} obtained from the radar and the model. Radar winds are smoothed over 1 h for comparison with the hourly model output.

Fig 7. Time-height section for Aberystwyth on 28 Oct 1996 derived from the MST radar and four mesoscale-model 6-hour forecast runs starting at 0,6,12 and 18 UTC. Colours represent log power received by the radar. The radar data were obtained at 12-min intervals and are unsmoothed to preserve fine structure. Superimposed lines represent the heights of the tropopause (white contour labelled 3) and the top of the moist boundary-layer air (white contour labelled 80) as inferred from the model-derived potential vorticity and relative humidity (with respect to ice where appropriate), respectively.

Fig 8 The 18 UTC radiosounding for Aberporth (near Aberystwyth) on 28 Oct 1996 superimposed on the model-derived sounding for the same time. Solid lines: temperature. Dashed lines: dew-point. Each wind barb (flag) represents 5 (25) ms^{-1} Thick lines: model-derived. Thin lines: from radiosonde.

Fig.9 Sequence of Meteosat infrared images showing the evolution of extratropical cyclone Lili during the generation of the hook cloud and eye while it was travelling across Ireland. (a) 09, (b)12, (c)15 and (d) 17 UTC, 28 Oct 1996.The grey shades represent brightness temperature according to the

scale. The part of the hook cloud that develops over Southern Ireland (b) and moves across the Irish Sea (c) and Wales (d) is referred to as a cloud head.

Fig.10. Weather radar network display showing the distribution of rainfall intensity over the British Isles at 15 UTC, 28 Oct 1996. The code for rainfall intensity is shown at the side of the display : the area of heaviest rain over the Irish Sea is up to 16 mm h^{-1}. The bold contours with partial hatching delineate the -15°C cloud-top boundary derived from Meteosat to show the association of the widespread moderately-heavy rain with the main hook cloud. Part of the hook cloud south and west of Ireland lies beyond radar range and the band of 'R's has been added to give a qualitative impression of the likely extent of rain, consistent with later observations made as the cyclone travelled eastwards.

Fig.11 Development of features related to the hook-and-eye structure as seen in sequences of data for 12 UTC (top row), 15 UTC (middle row) and 17 UTC, 28 Oct 1996 (bottom row). Left-hand (a) and middle column (b) : Potential vorticity at 900 and 400 hPa, respectively, as derived from the 12 UTC forecast run of the operational mesoscale model. Lightly and heavily shaded areas in (a) correspond to PV>2 and 1, respectively. In (b) the shaded areas correspond to PV>2. L marks the centre of cyclone Lili at the surface. The dashed line SS representing the axis of the PV anomaly at 700 hPa is referred to in the text in Sec. 4(b and c). Right-hand column(c) : Extent of hook cloud with T_B< -25°C derived from the satellite imagery in Fig 9.

Fig. 12 Analyses from the operational run of the mesoscale model at 12 UTC, 28 Oct 1996 at 400 (top), 700 (middle) and 900 hPa (bottom row). Left column (a) shows dry-bulb potential

temperature, with isotherms at 1°C intervals and darker shading representing warmer regions. Right column (b) shows the magnitude of the vector wind velocity, with isotachs at 2 ms^{-1} intervals, and darker shading representing higher speeds. The dashed curved lines around Ireland represent the axis of maximum speed associated with the cyclone at each level, and the long dashed curves extending northeastwards from the English Channel represent the corresponding axis of maximum speed associated with the upper-level jet. AA' shows the position of the vertical section in Figs. 13 and 14.

Fig 13.

Mesoscale model output for a vertical section along AA' in Fig.12 at 15 UTC 28 Oct 1996 from the operational forecast run made at 12 UTC. (a) : wet-bulb potential temperature (solid isopleths at 0.5°C intervals; increasingly dark shading for higher values)and dry-bulb potential temperature (dashed isopleths at 10 K intervals). (b) : magnitude of the vector wind velocity (isopleths at 5 ms^{-1} intervals; increasingly dark shading for higher speeds). Upper-level and lower-level jet axes are labelled J_u and J_L, respectively. The dashed line is the axis of minimum velocity, with winds to the left (northwest) of the axis having a northerly component and those to the right a southerly component. (c) : potential vorticity (isopleths at intervals of 0.5 pv unit; increasingly dark shading for values in excess of 1.5 pvu). The dashed line SS is the axis of the PV streamer emanating from the tropopause fold. (d) : relative humidity (with respect to ice where appropriate) (isopleths at intervals of 10%; increasingly dark shading for values in excess of 40%).

Fig.14. Synthesis of information from Fig. 13 (a - d) depicting the structure of cyclone Lili at 15 UTC, 28 Oct 1966. The thin solid line and stippled shading represents wet-bulb potential temperature ≥ 12°C from Fig. 13(a). This is terminated at 500 hPa and capped by a perspective-view lid to give a 3-D impression. J_u and J_L, respectively, denote the upper- and lower-level jet axes from Fig.13(b); the perspective-view partial circles show the two low-level jets as part of the same cyclone vortex, the axis of which is given by the dashed line. The bold line is a slightly schematicized version of the dynamic tropopause corresponding to the PV = 2 isopleth in Fig. 13(c) . The dashed line SS corresponds to the axis of high PV within the troposause fold and the region of horizontal hatching represents the diabatically generated region of PV ≥ 2 pv units. The wavy line corresponds to the model's RH = 80% isopleth which we interpret as corresponding roughly to the top of the actual region of cloud.

Fig. 15 Aspects of the structure of the dry intrusion at15 UTC, 28 Oct 1996, derived from the 12 UTC operational forecast run of the mesoscale model. (a): Axes of maximum PV at various levels to show the overall configuration of the PV streamer labelled SS in Fig.13(c). AA' shows the position of the section in Fig.13. The axis of the PV anomaly at 300 hPa is shown by the line of circles: axes at 400, 500, 600 and 700 hPa are shown by solid, long-dashed, short-dashed and dotted lines, respectively. The shaded area, representing PV> 1.5 at 500 hPa, shows the top of the diabatically generated PV column. (b), (c) and (d): plan sections at 700 hPa showing PV at intervals of 0.25 PV units, relative humidity at intervals of 10% and wet-bulb potential temperature at intervals of 1K, respectively: in each case increasingly dark shading is used for higher values. The dashed

curve, plotted in the same location in (b), (c) and (d), represents the nominal axis of the dry intrusion at 700 mb

Fig.16. Extent of air with a wet-bulb potential temperature (θ_w) of 12°C, drawing attention to the penetration of low -θ_w air into the cyclone eye at (a) 12 UTC, (b) 15 UTC and (c) 17 UTC, 28 Oct 1996, as derived from the 12 UTC operational forecast run of the mesoscale model. Dark shading is for 700 hPa. Solid contours are for 800 hPa; and dashed contours are for 900 hPa.

Fig 17. Schematic representation of the structure of the mature warm-core extratropical cyclone Lili, at approx 15 UTC, 28 Oct 1996, showing cut-away views of aspects of its horizontal and vertical structure. Vertical-line shading draws attention to moist/cloudy regions within a vertical section orientated northwest-to-southeast (NW-SE) (the cyclone's direction of travel is roughly west-to-east). Thin radial lines draw attention to the 700-hPa top of a cut-away part of a cylinder representing the cyclone's vortex, characterised by a strong low-level jet (LLJ) especially on the southern side. The hatched ribbon within the NW-SE section represents the tropopause; this descends as a fold toward the cloud head at the leading edge of the hook cloud. The 3 tubular arrows starting at the southwestern end of the SW-NE section, show the stratospheric, transitional and tropospheric parts of a continuous dry-intrusion flow that was descending around the cloud head. The tropospheric part of the dry intrusion (lower 2 tubular arrows) penetrates into the eye region after a 270-degree circuit around the cloud head. Only a portion of the stratospheric part of the dry intrusion (topmost tubular arrow) circulates around the cloud head; the rest of the stratospheric air carries on past the cyclone.

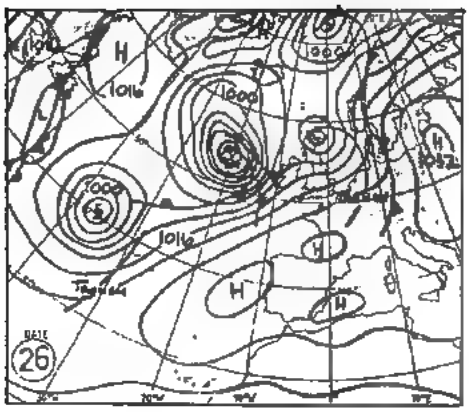
H
1016
1000
1016
H
H
H
DATE
26

(a)

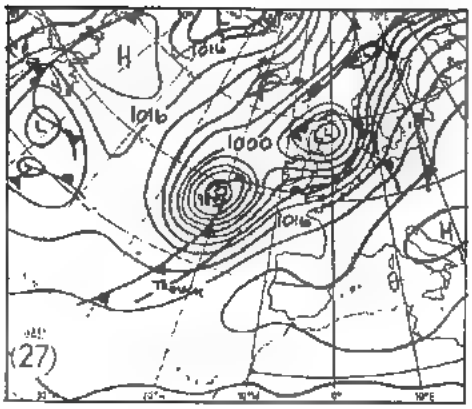
H
1016
1000
1016
H
DATE
27

(b)

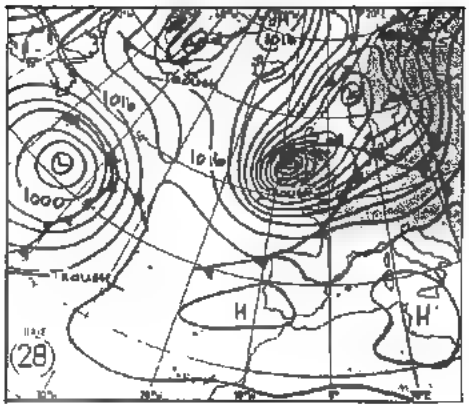
1016
1016
1000
H
H
DATE
28

(c)

Figure 1

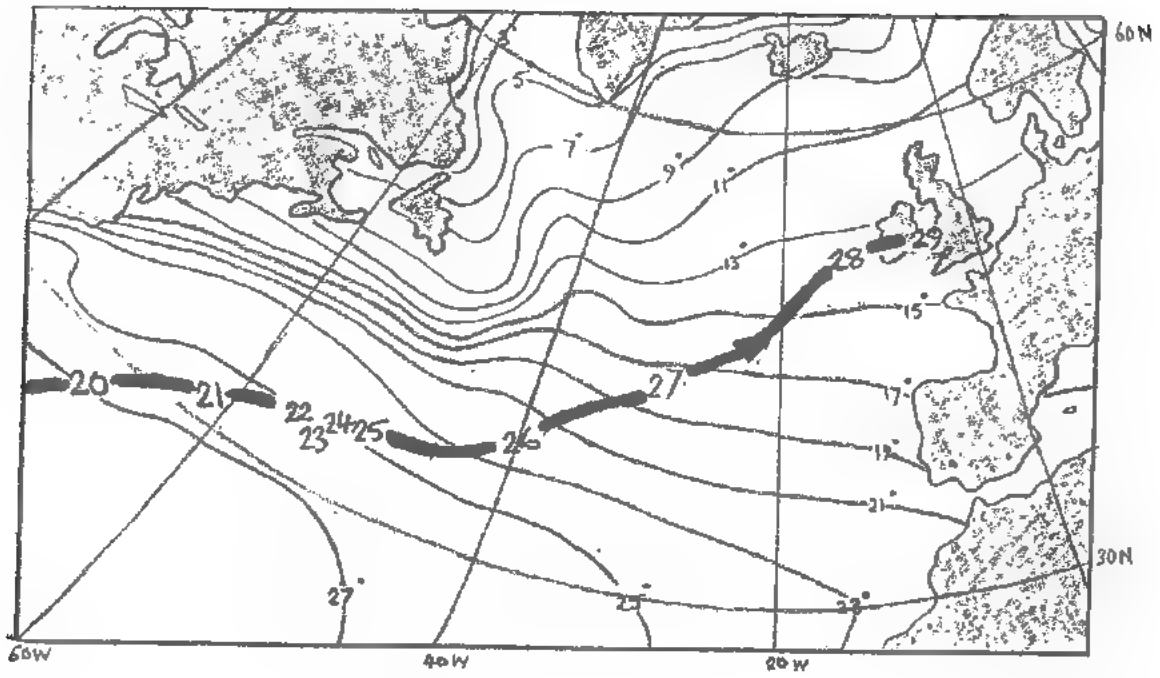
60N
30N
60W
40W
20W
5
7
9
11
13
15
17
19
21
27
25
29
28
27
20
21
22
23
24
25
26

Figure 2

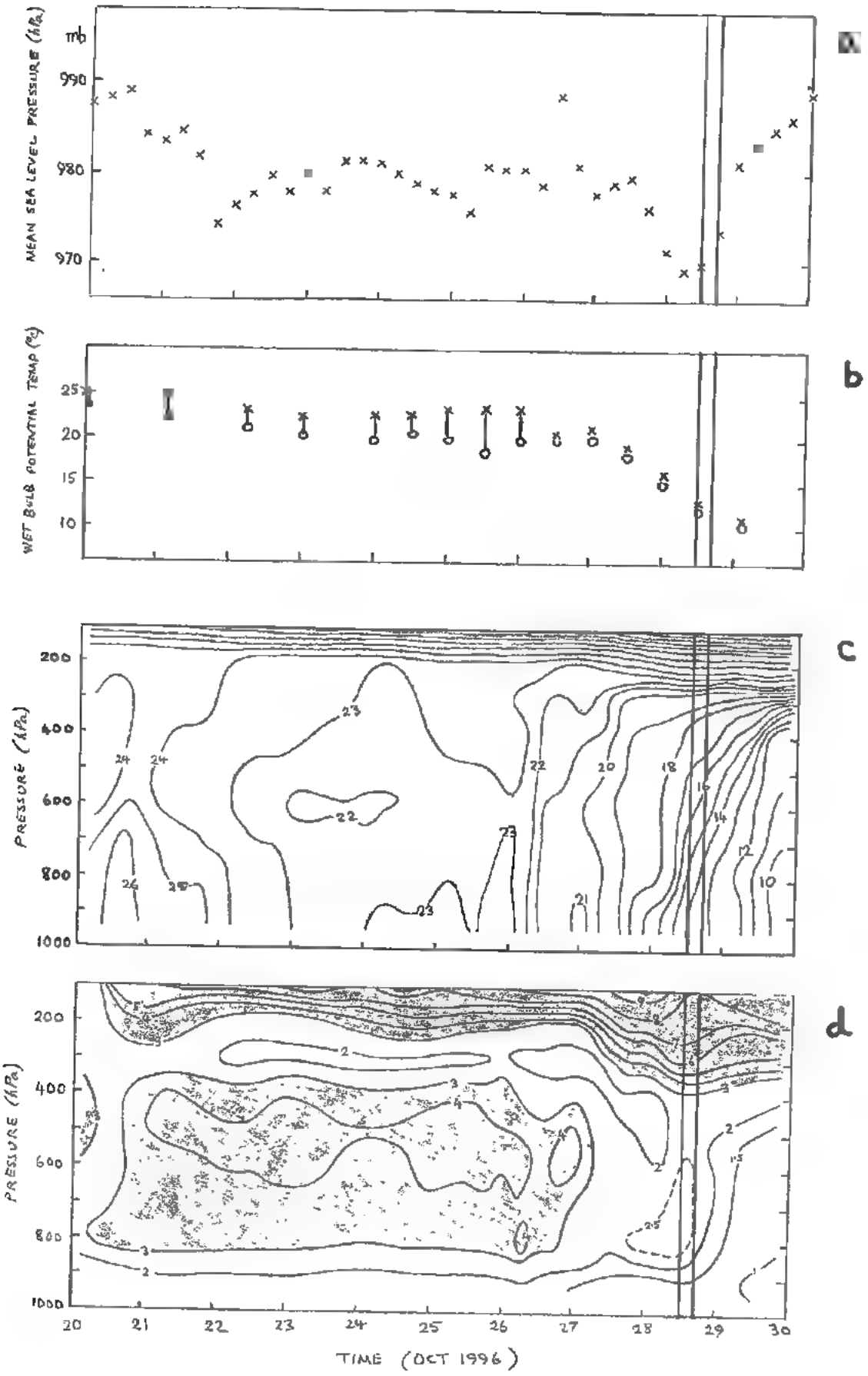
a
MEAN SEA LEVEL PRESSURE (hPa)
mb
990
980
970
b
WET BULB POTENTIAL TEMP (°C)
25
20
15
10
c
PRESSURE (hPa)
200
400
600
800
1000
24
23
22
21
20
18
16
14
12
10
d
PRESSURE (hPa)
200
400
600
800
1000
20
21
22
23
24
25
26
27
28
29
30
TIME (OCT 1996)

Fig 3

AAAAD 41 theta-w at 900.0 nPa

a At 00Z on 26/10/1996

AAAAD 41 theta-w at 900.0 hPa

b

AAAAD 41 theta -w at 900.0 nPa

c At 00Z on 28/10/1996

Fig 4

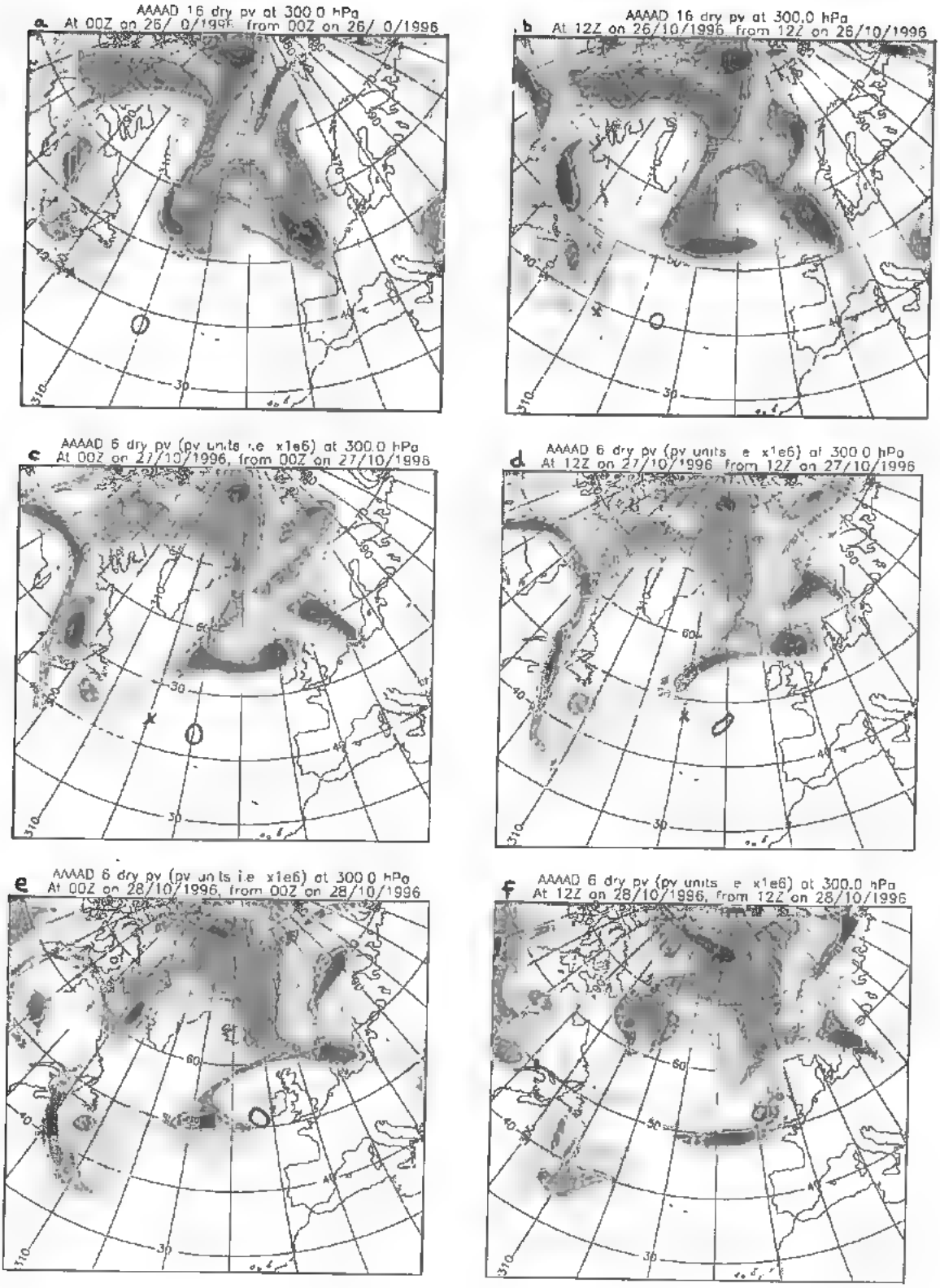
a
AAAAD 16 dry pv at 300.0 hPa
At 00Z on 26/ 0/1996 from 00Z on 26/ 0/1996
b
AAAAD 16 dry pv at 300.0 hPa
At 12Z on 26/10/1996 from 12Z on 26/10/1996
c
AAAAD 6 dry pv (pv units i.e x1e6) at 300.0 hPa
At 00Z on 27/10/1996, from 00Z on 27/10/1996
d
AAAAD 6 dry pv (pv units i.e x1e6) at 300.0 hPa
At 12Z on 27/10/1996 from 12Z on 27/10/1996
e
AAAAD 6 dry pv (pv units i.e x1e6) at 300.0 hPa
At 00Z on 28/10/1996, from 00Z on 28/10/1996
f
AAAAD 6 dry pv (pv units i.e x1e6) at 300.0 hPa
At 12Z on 28/10/1996, from 12Z on 28/10/1996

Fig 5

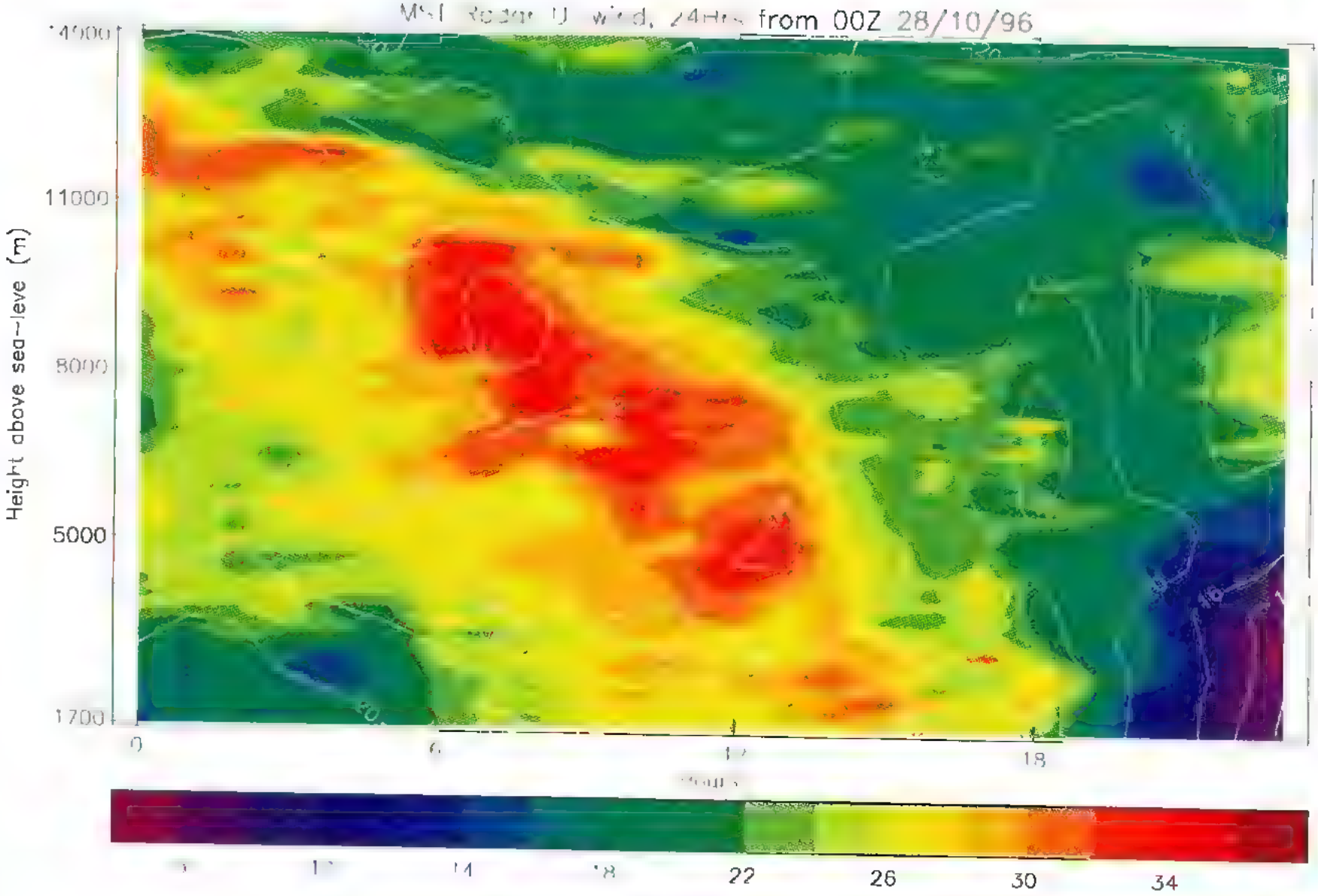
from 00Z 28/10/96
Height above sea-leve (m)
11000
8000
5000
1700
0
6
18
22
26
30
34

Fig 6(a)

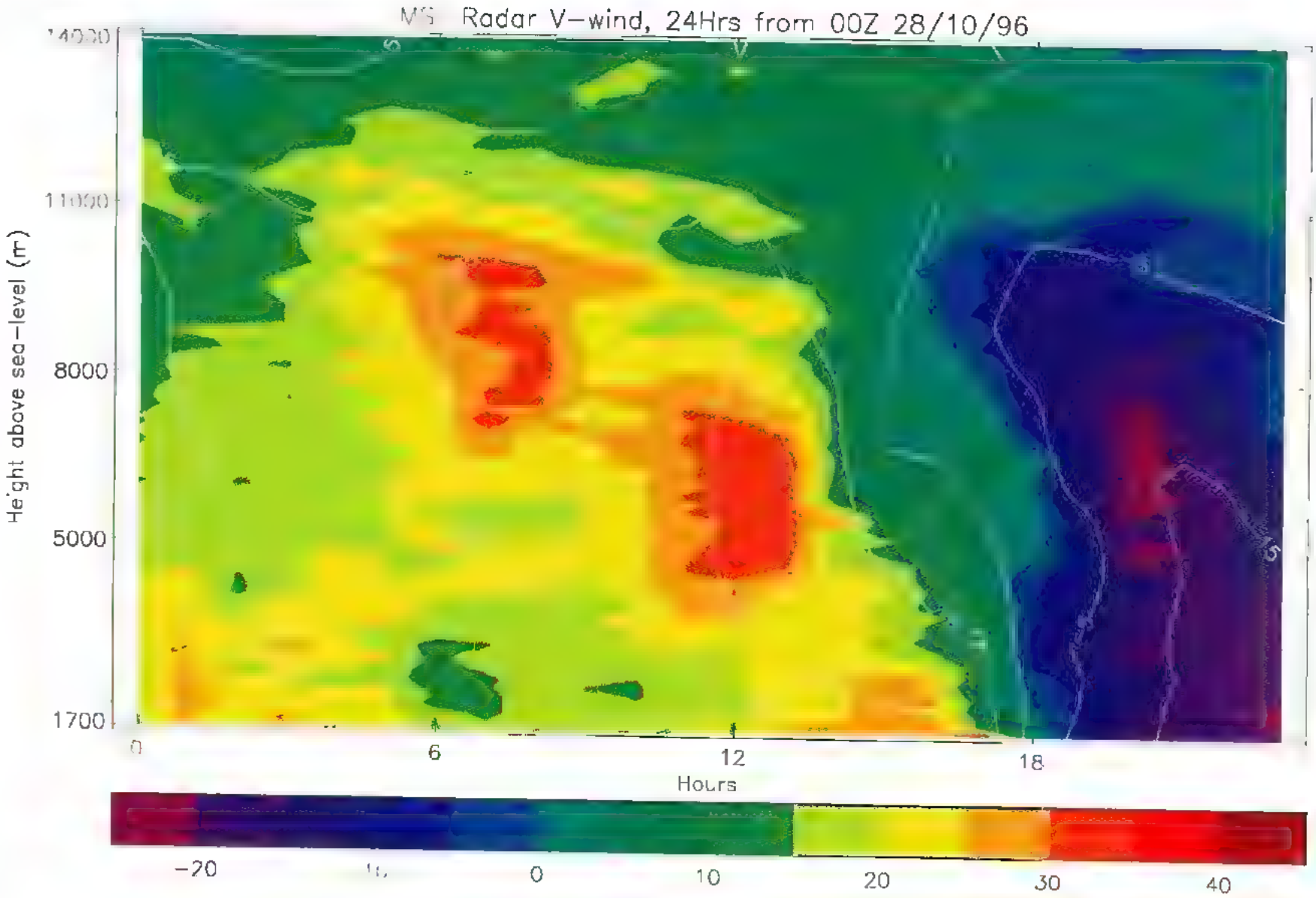
MS Radar V-wind, 24Hrs from 00Z 28/10/96
14000
11000
8000
5000
1700
Height above sea-level (m)
0
6
12
18
Hours
-20
0
10
20
30
40

Fig 6(b)

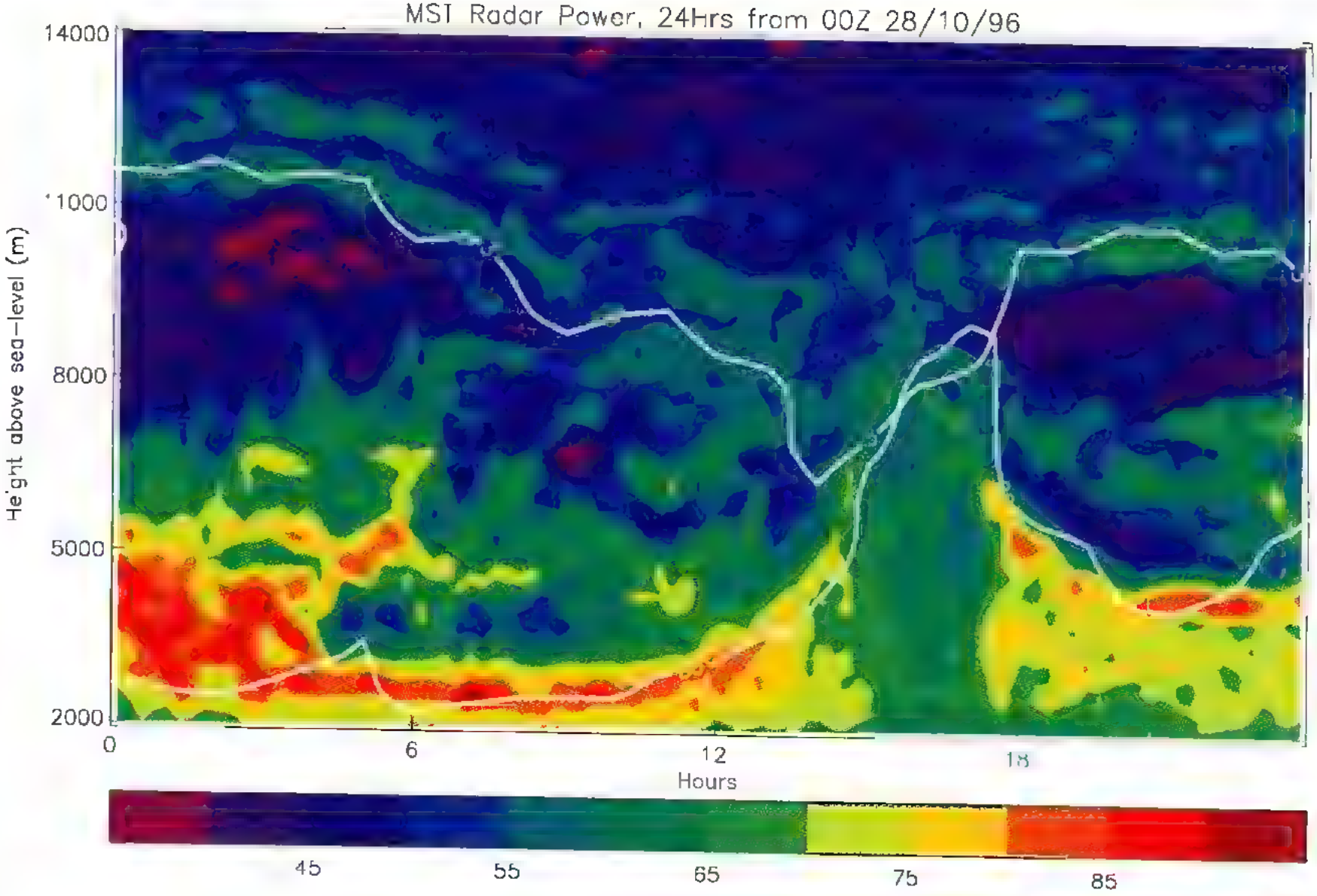
MST Radar Power, 24Hrs from 00Z 28/10/96
14000
11000
8000
5000
2000
Height above sea-level (m)
0
6
12
18
Hours
45
55
65
75
85

Fig 7

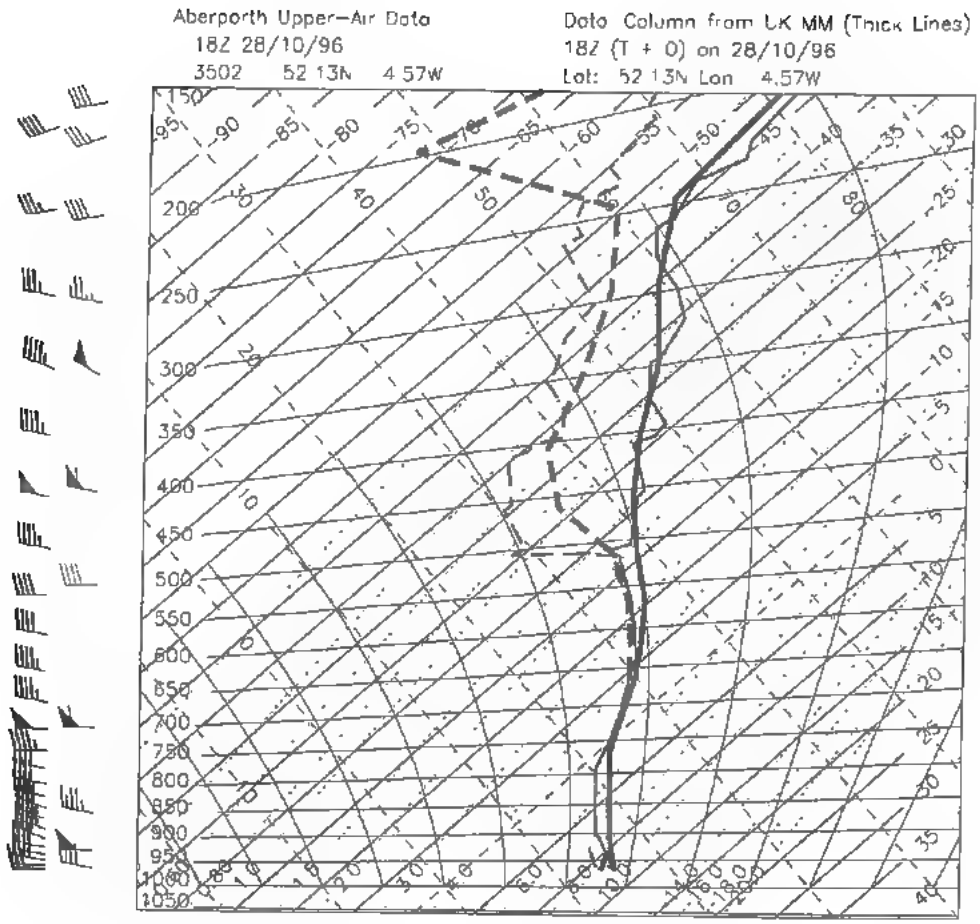
Aberporth Upper-Air Data
18Z 28/10/96
3502 52 13N 4 57W
Data Column from UK MM (Thick Lines)
18Z (T + 0) on 28/10/96
Lat: 52 13N Lon 4.57W

Fig.8

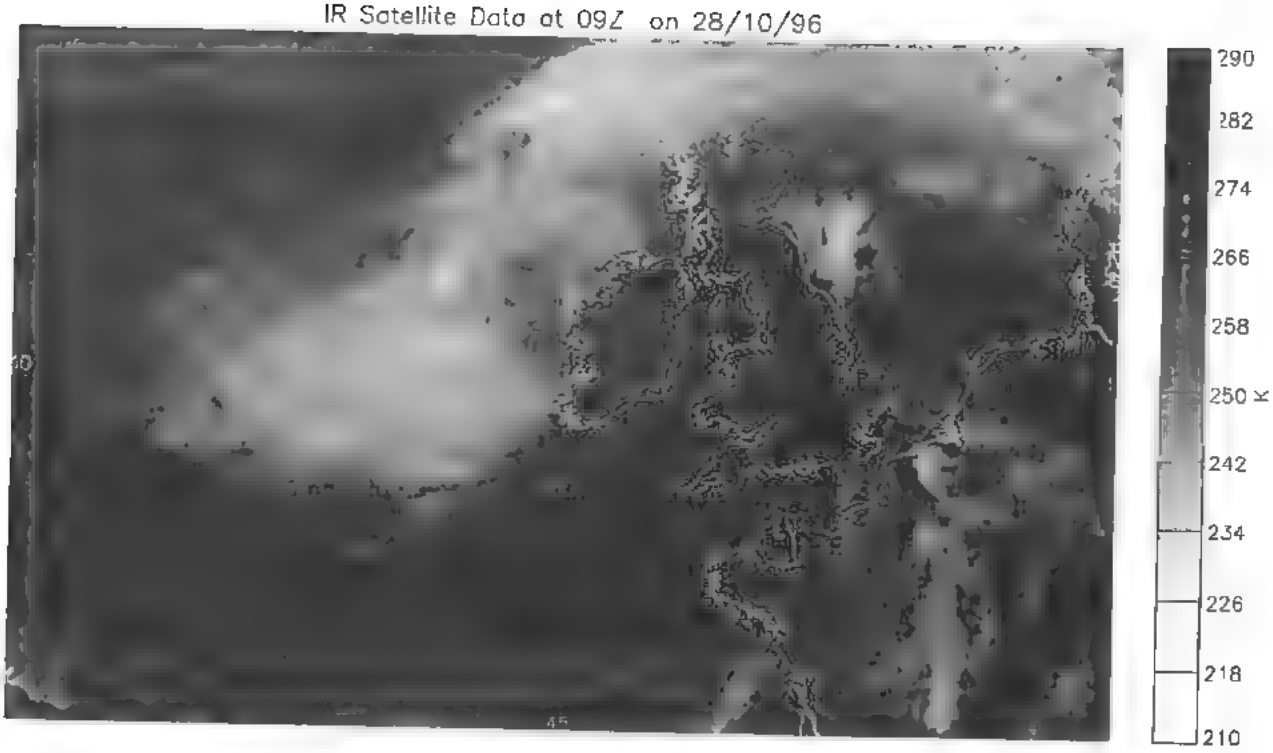
IR Satellite Data at 09Z on 28/10/96
290
282
274
266
258
250 K
242
234
226
218
210

Fig 9(a)

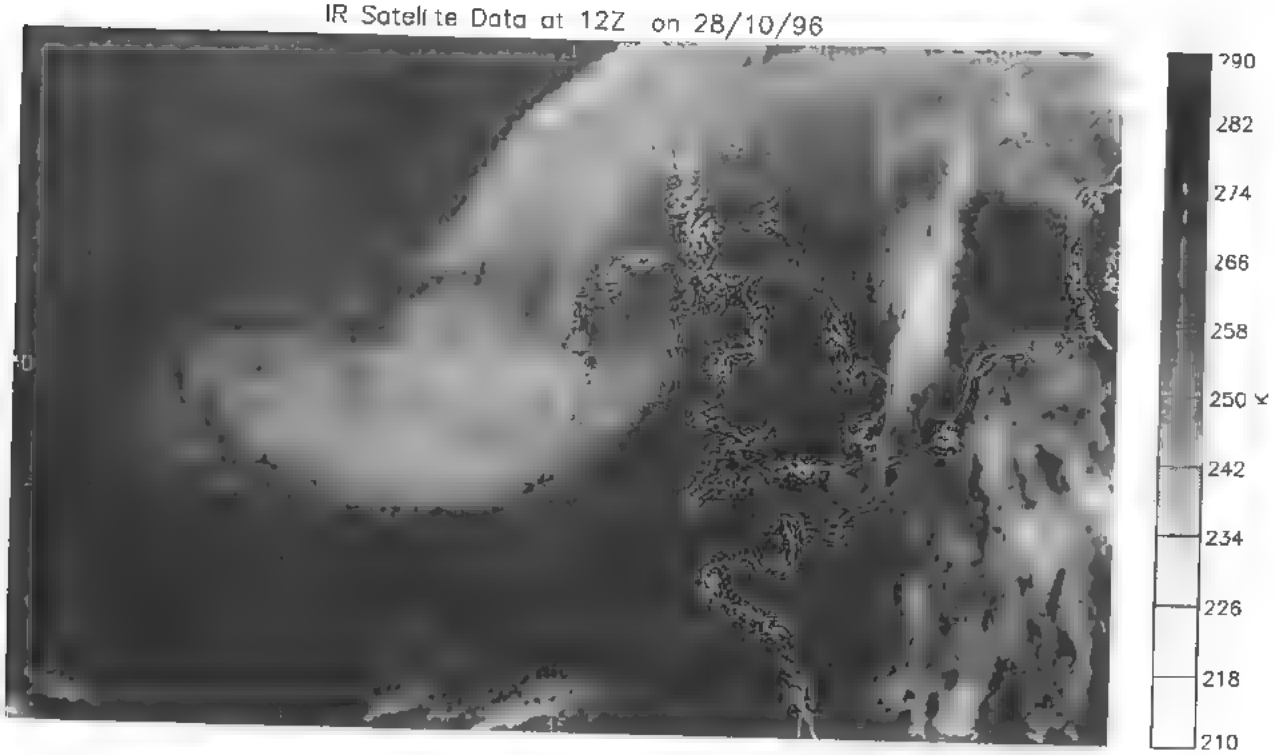
IR Satellite Data at 12Z on 28/10/96
290
282
274
266
258
250 K
242
234
226
218
210

Fig 9(b)

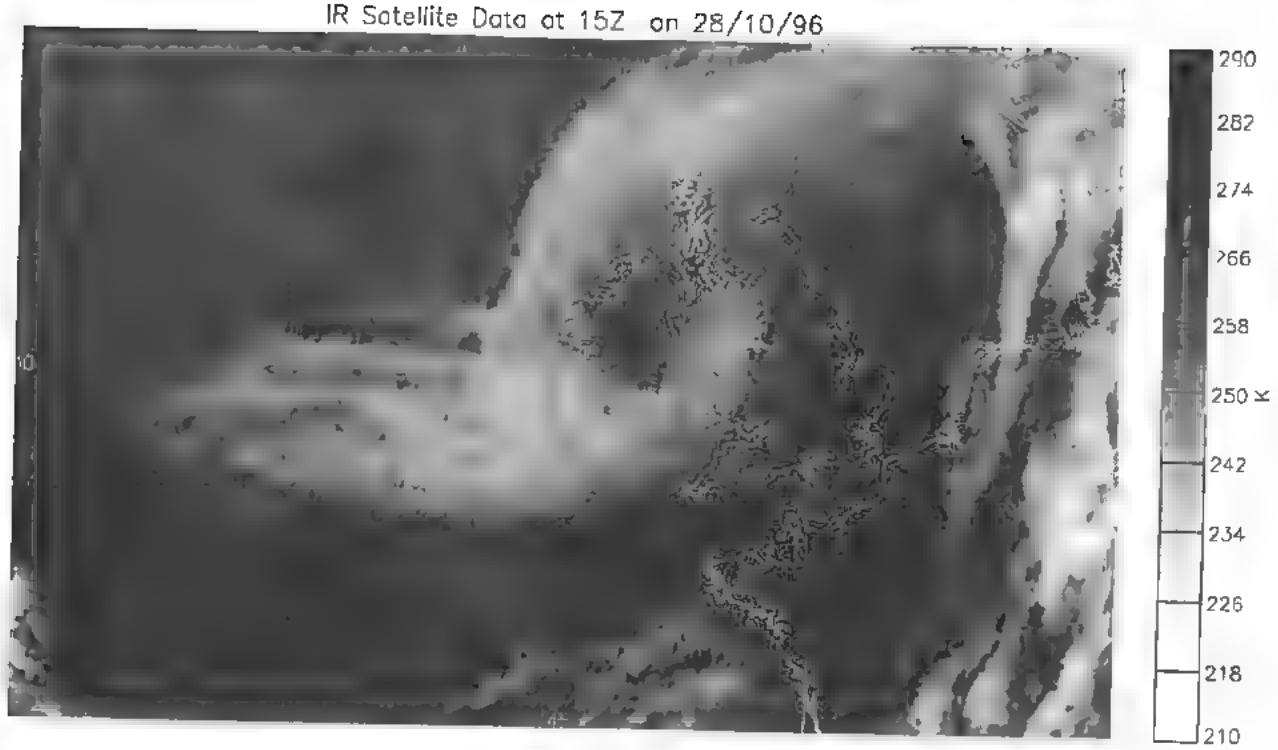
IR Satellite Data at 15Z on 28/10/96
290
282
274
266
258
250 K
242
234
226
218
210

Fig 9(c)

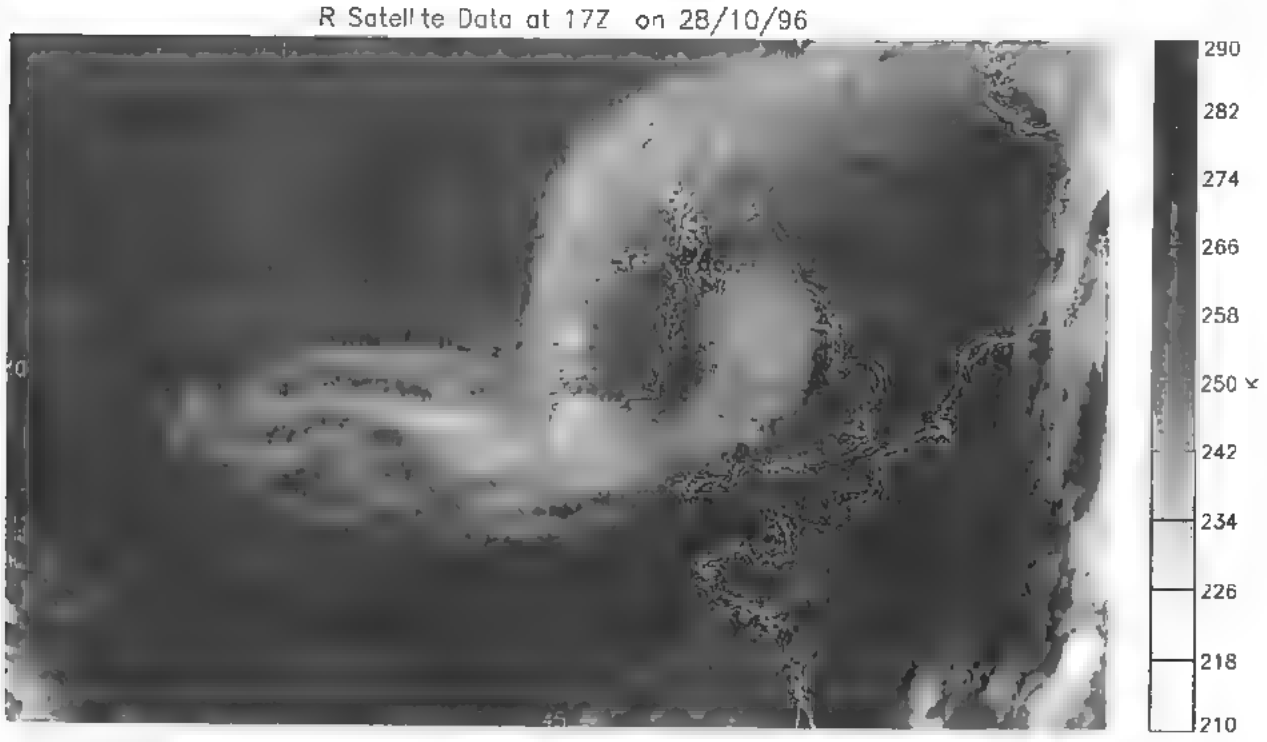
R Satellite Data at 17Z on 28/10/96
290
282
274
266
258
250 K
242
234
226
218
210

Fig 9(d)

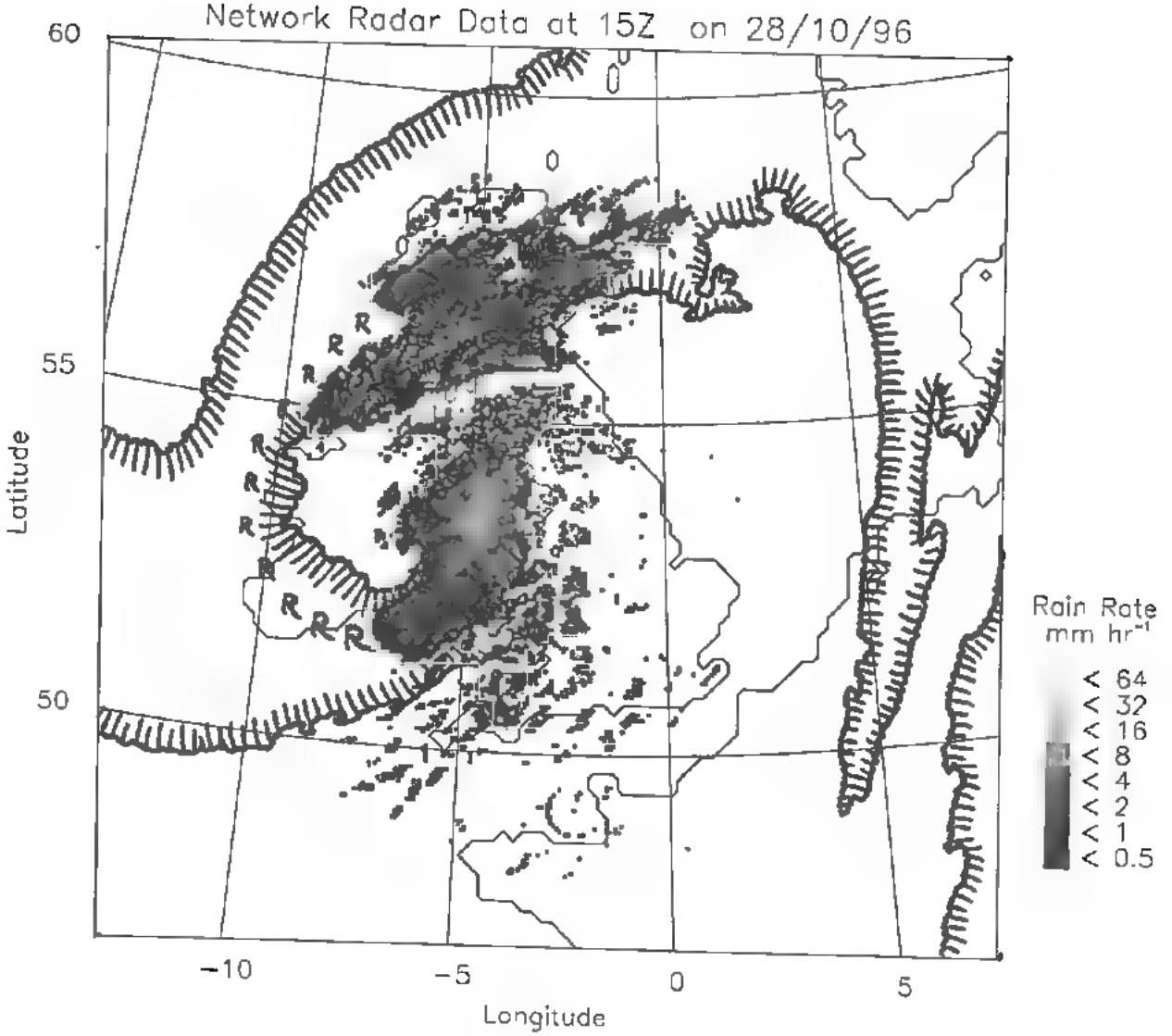
Network Radar Data at 15Z on 28/10/96
60
55
50
Latitude
−10
−5
0
5
Longitude
Rain Rate
mm hr⁻¹
< 64
< 32
< 16
< 8
< 4
< 2
< 1
< 0.5

Fig. 10

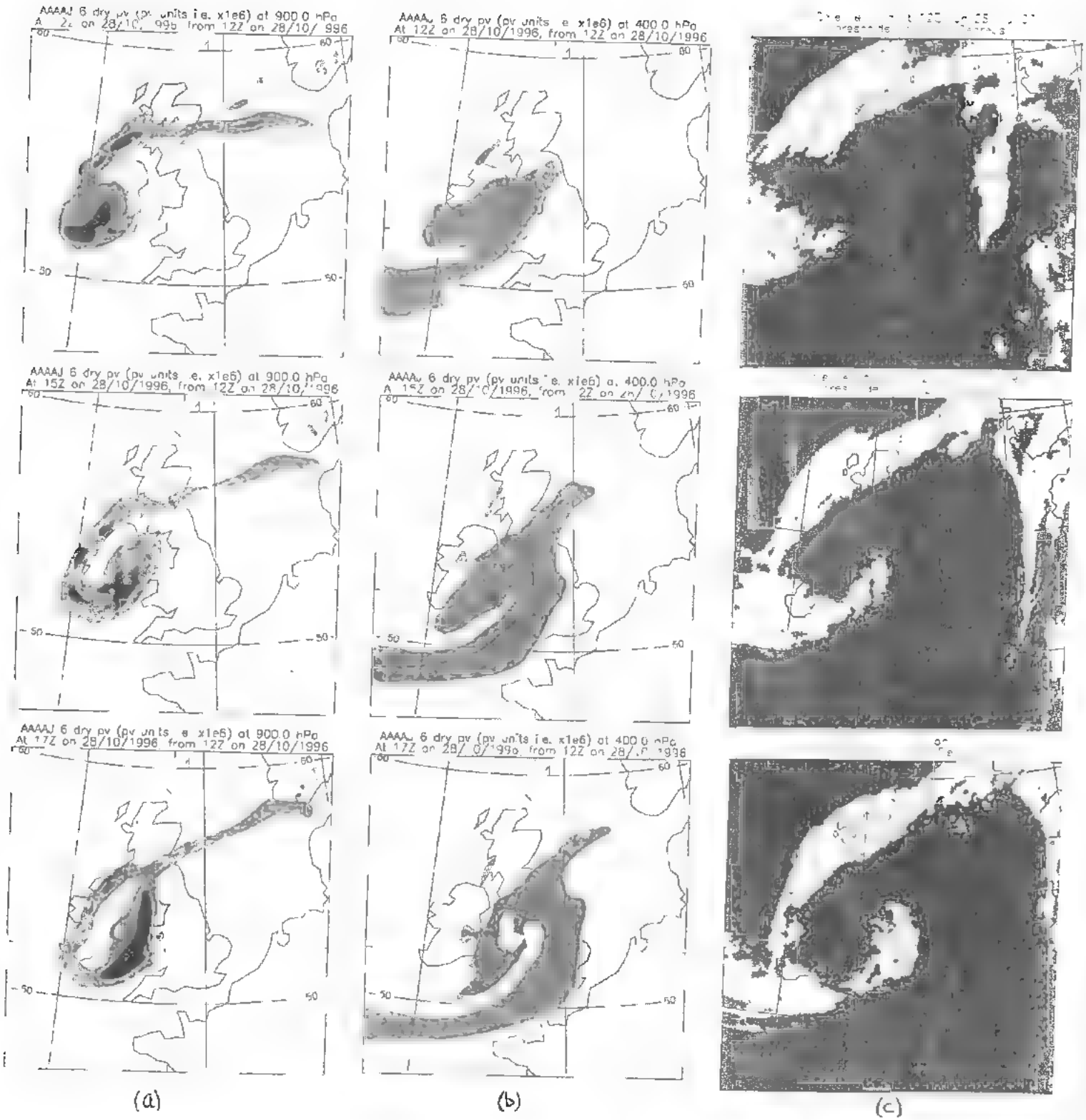

Fig 11

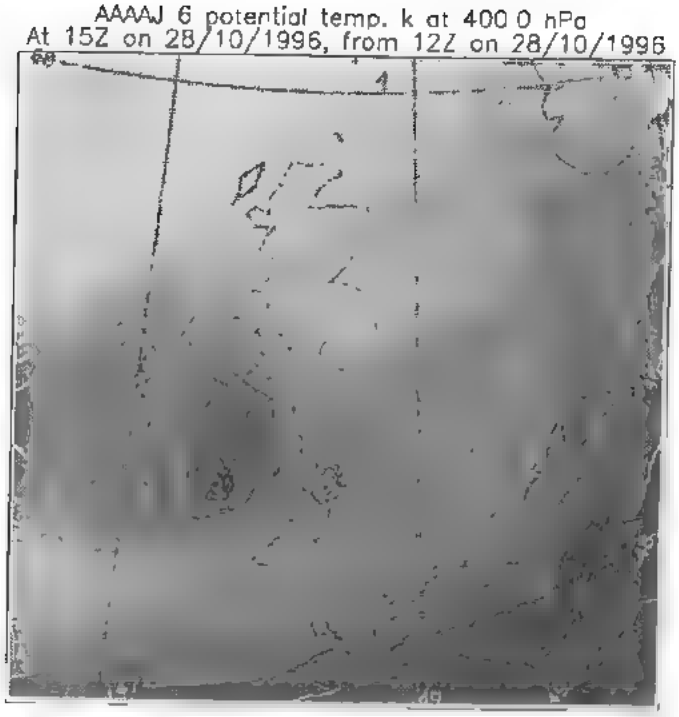
AAAAJ 6 potential temp. k at 400.0 hPa
At 15Z on 28/10/1996, from 12Z on 28/10/1996

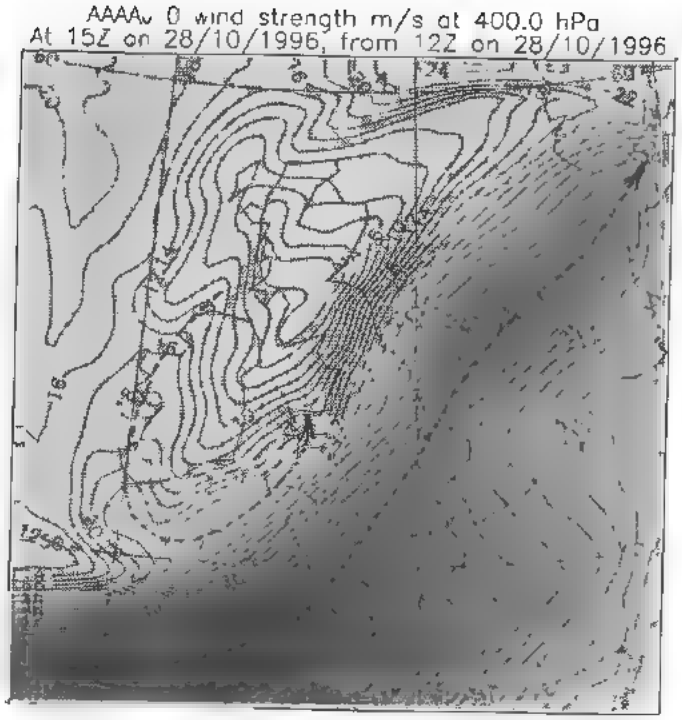
AAAA 0 wind strength m/s at 400.0 hPa
At 15Z on 28/10/1996, from 12Z on 28/10/1996

Figure 12

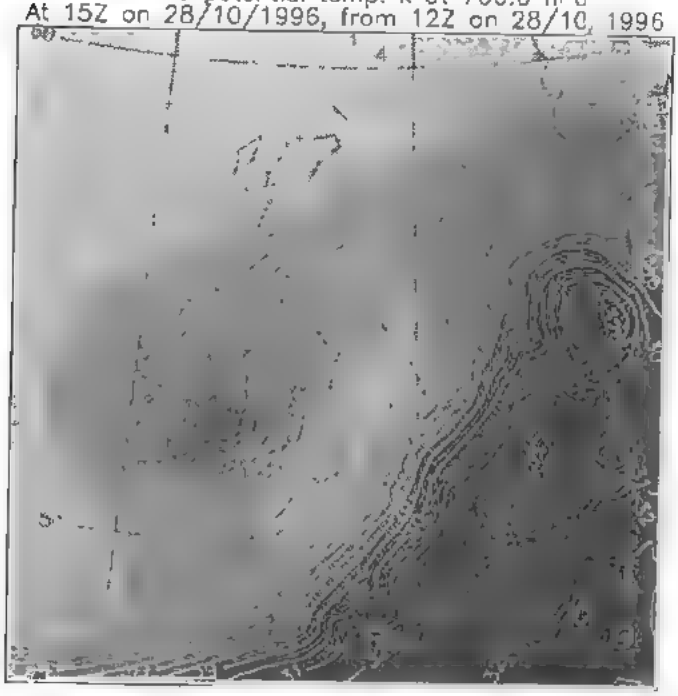
AAAAJ 6 potential temp. k at 700.0 hPa
At 15Z on 28/10/1996, from 12Z on 28/10, 1996

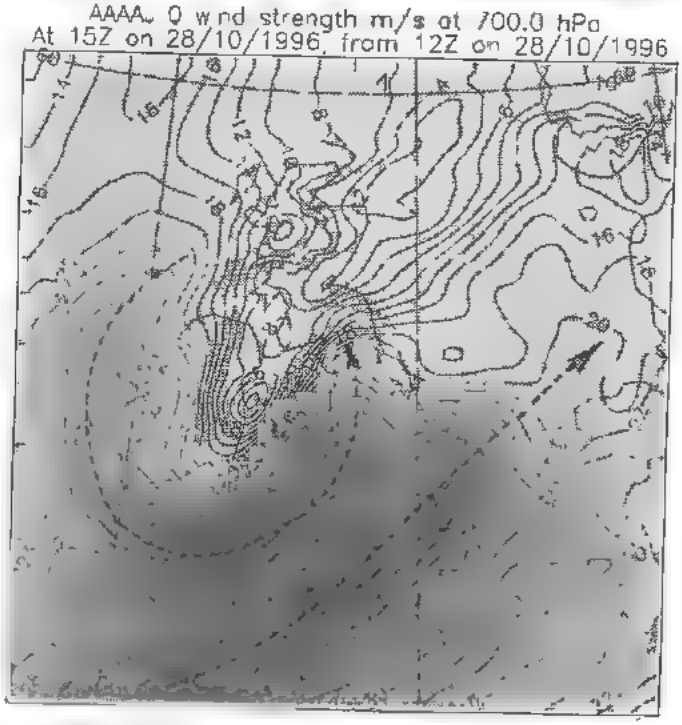
AAAA 0 wind strength m/s at 700.0 hPa
At 15Z on 28/10/1996, from 12Z on 28/10/1996

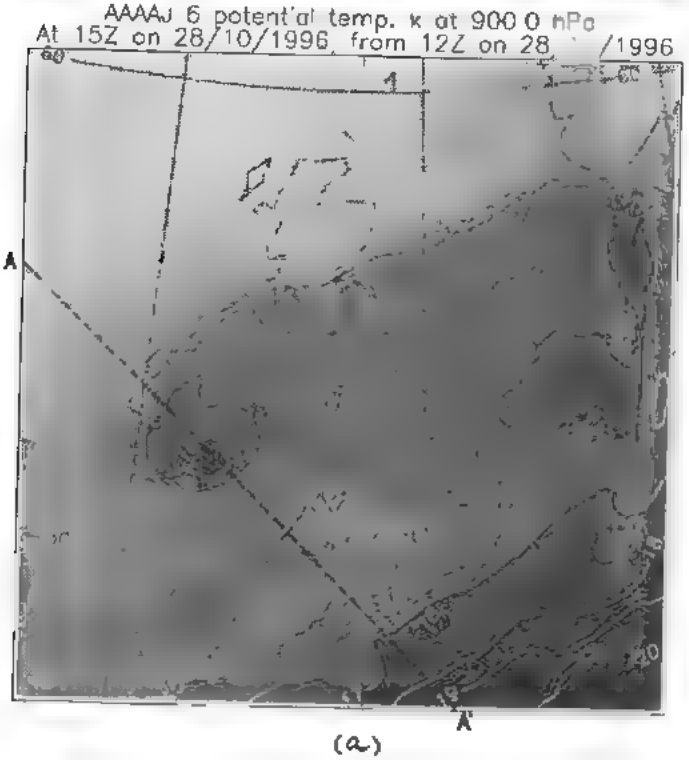
AAAAJ 6 potential temp. k at 900.0 hPa
At 15Z on 28/10/1996, from 12Z on 28 /1996
A
A'

(a)

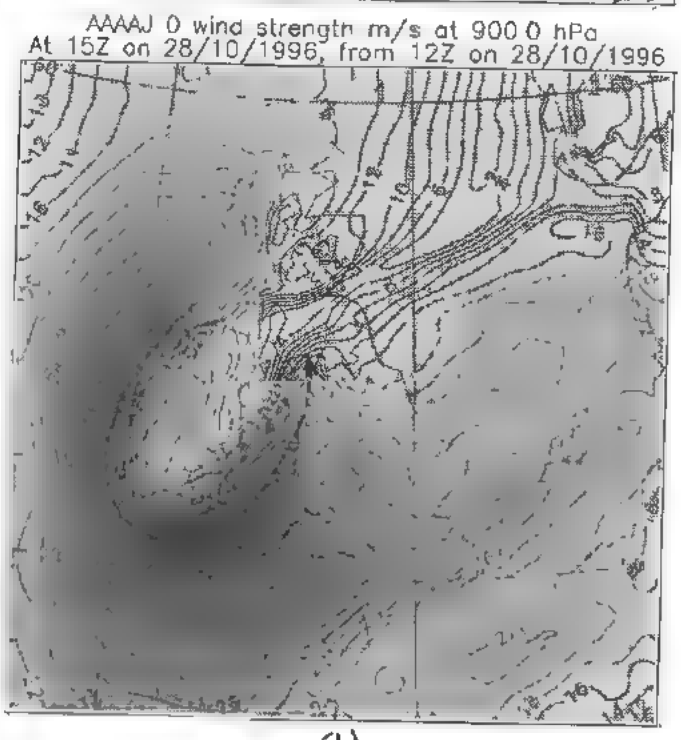
AAAAJ 0 wind strength m/s at 900.0 hPa
At 15Z on 28/10/1996, from 12Z on 28/10/1996

(b)

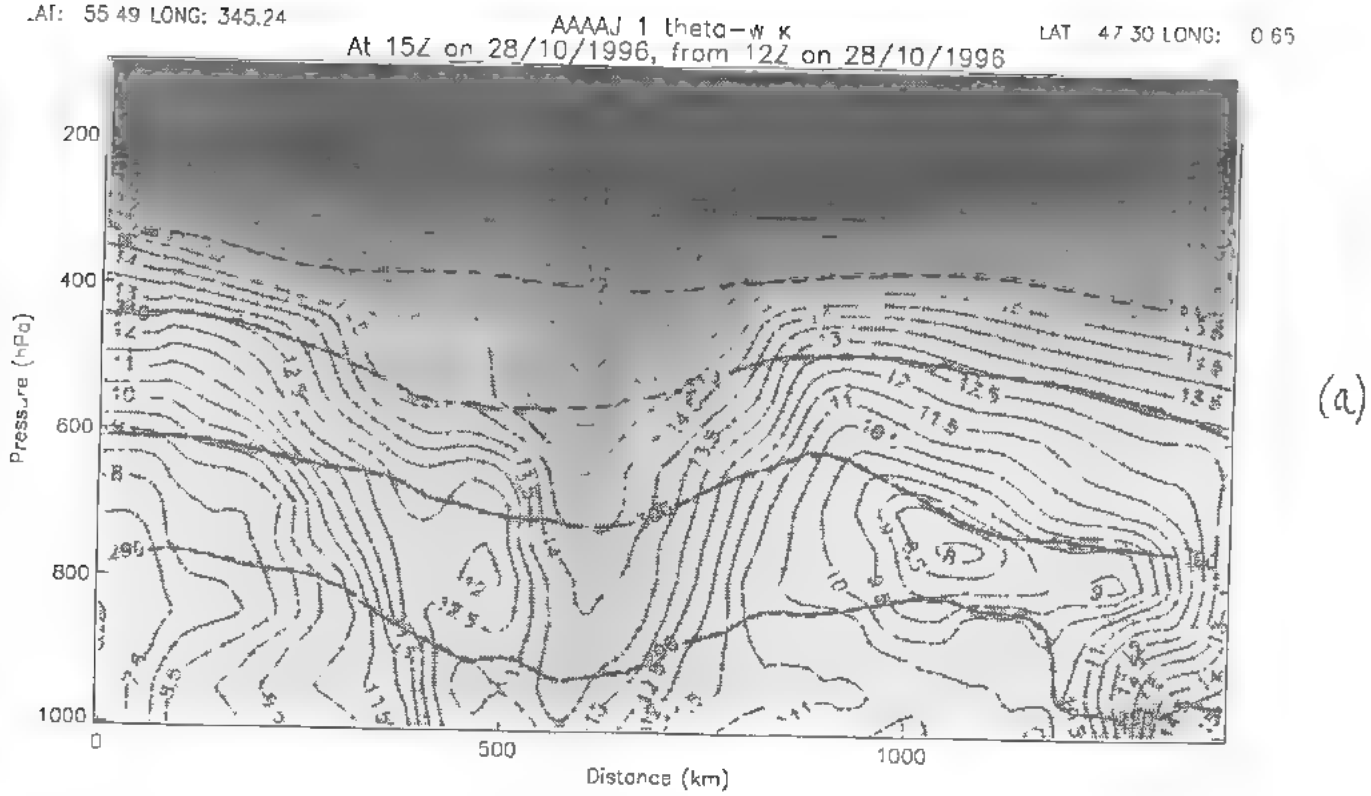
LAT: 55 49 LONG: 345.24
AAAAJ 1 theta-w K
At 15Z on 28/10/1996, from 12Z on 28/10/1996
LAT 47 30 LONG: 0 65
Pressure (hPa)
200
400
600
800
1000
0
500
1000
Distance (km)

(a)

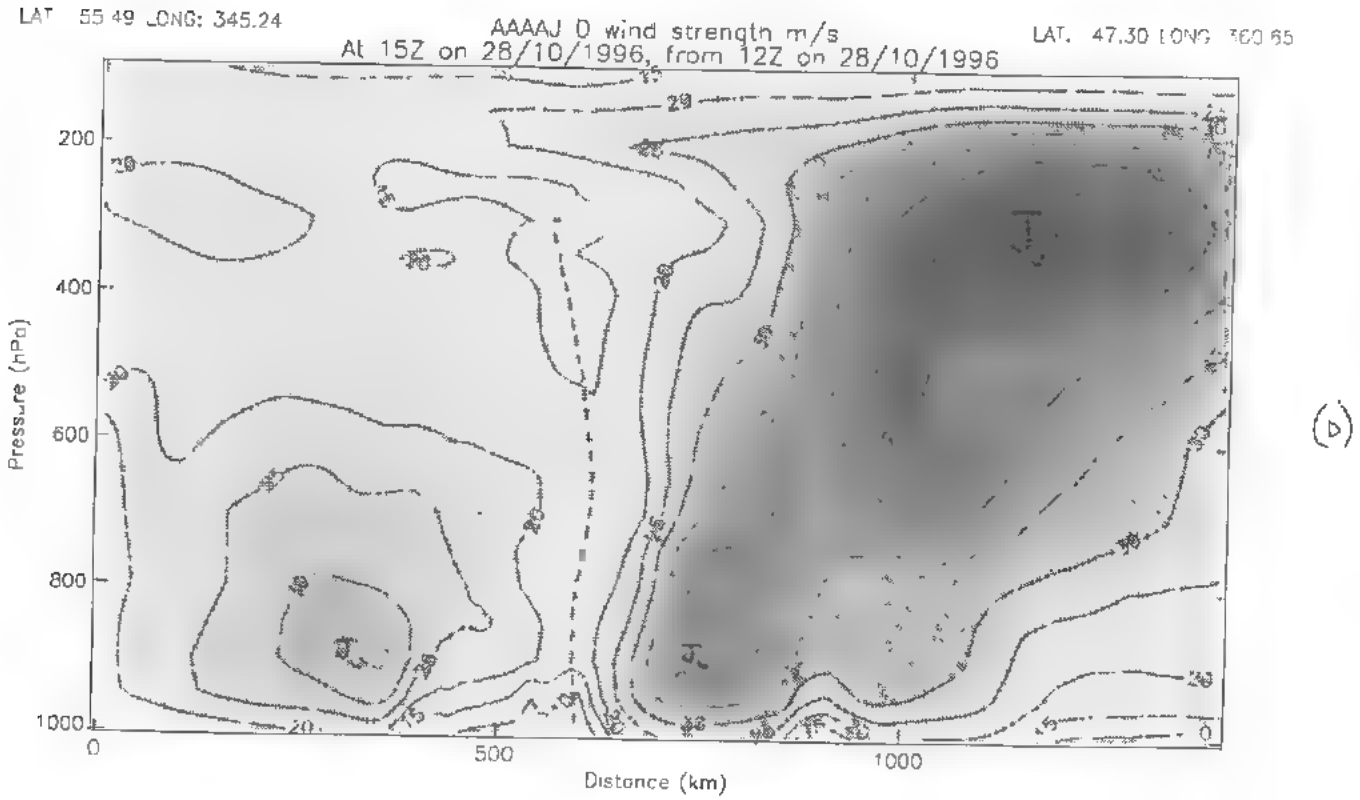
LAT 55 49 LONG: 345.24
AAAAJ 0 wind strength m/s
At 15Z on 28/10/1996, from 12Z on 28/10/1996
LAT. 47.30 LONG 360 65
Pressure (hPa)
200
400
600
800
1000
0
500
1000
Distance (km)

(b)

Fig 13

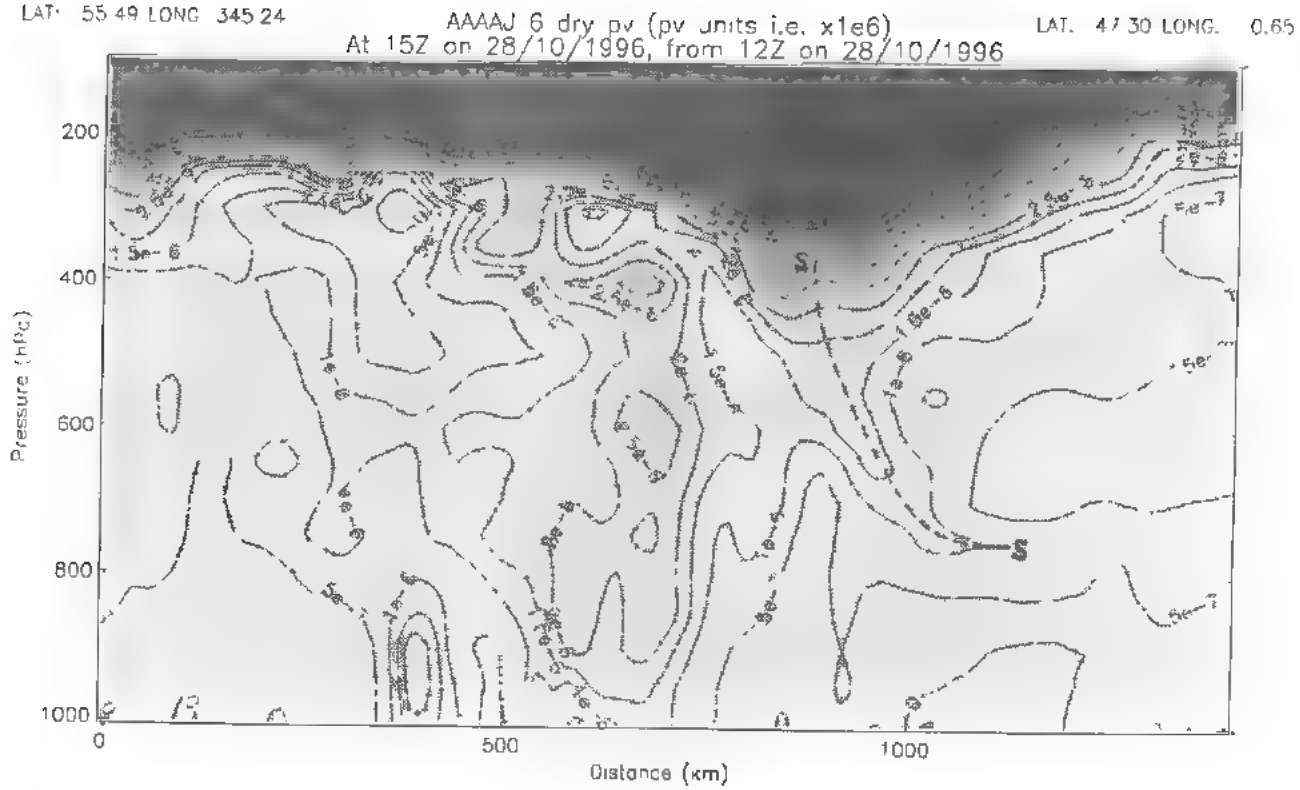
LAT 55.49 LONG 345.24
AAAAJ 6 dry pv (pv units i.e. x1e6)
At 15Z on 28/10/1996, from 12Z on 28/10/1996
LAT 47.30 LONG 0.65
Pressure (hPa)
200
400
600
800
1000
0
500
1000
Distance (km)
S
(c)

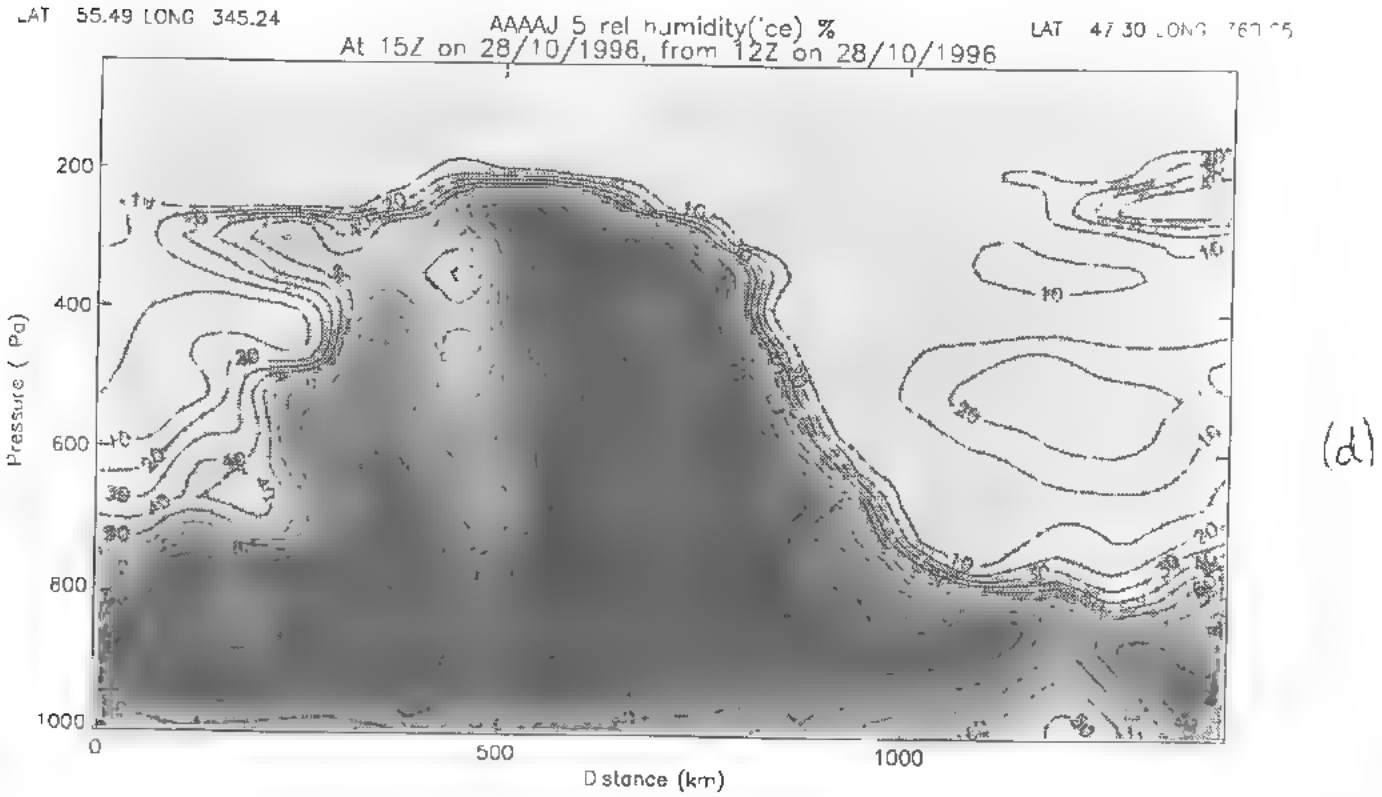
LAT 55.49 LONG 345.24
AAAAJ 5 rel humidity(ice) %
At 15Z on 28/10/1996, from 12Z on 28/10/1996
LAT 47.30 LONG 0.65
Pressure (Pa)
200
400
600
800
1000
0
500
1000
Distance (km)
(d)

Fig 13

Fig 14

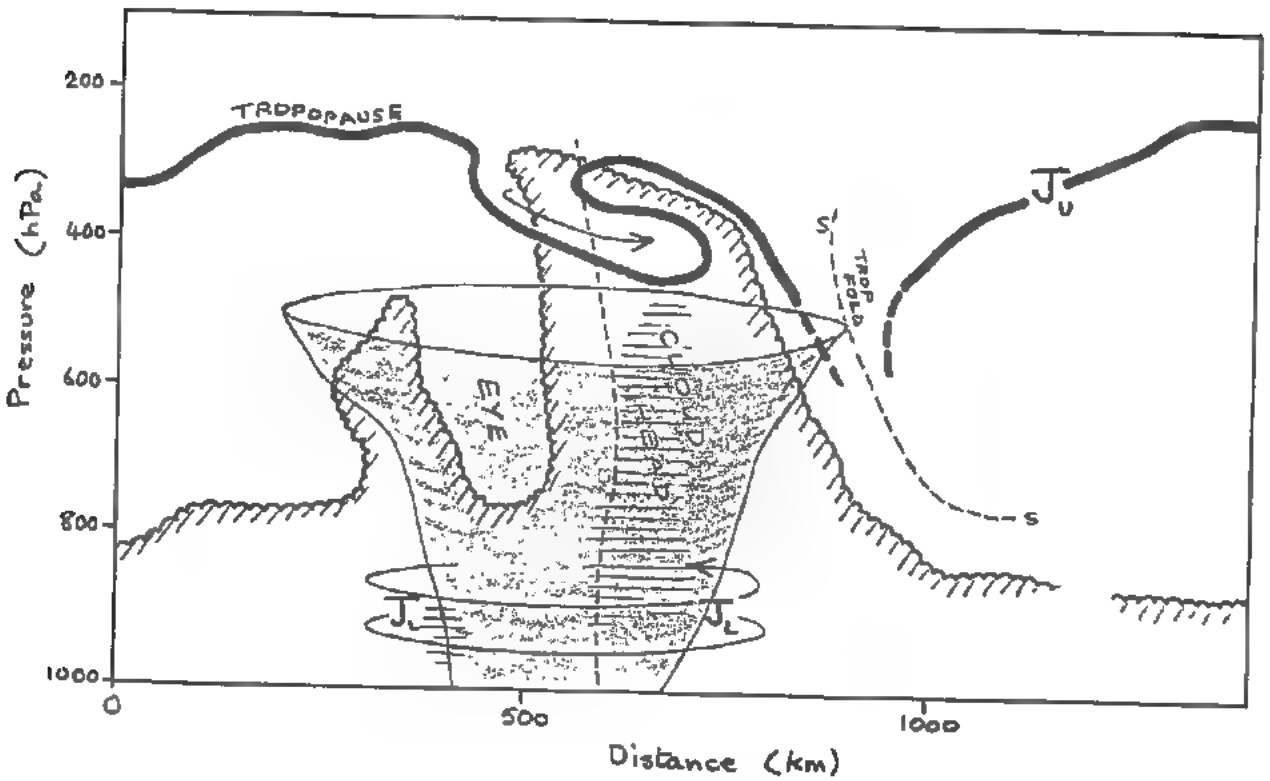
200
400
600
800
1000
Pressure (hPa)
TROPOPAUSE
EYE
CLOUD BAND
J_U
S
TROP FOLD
s
J_L
J_L
0
500
1000
Distance (km)

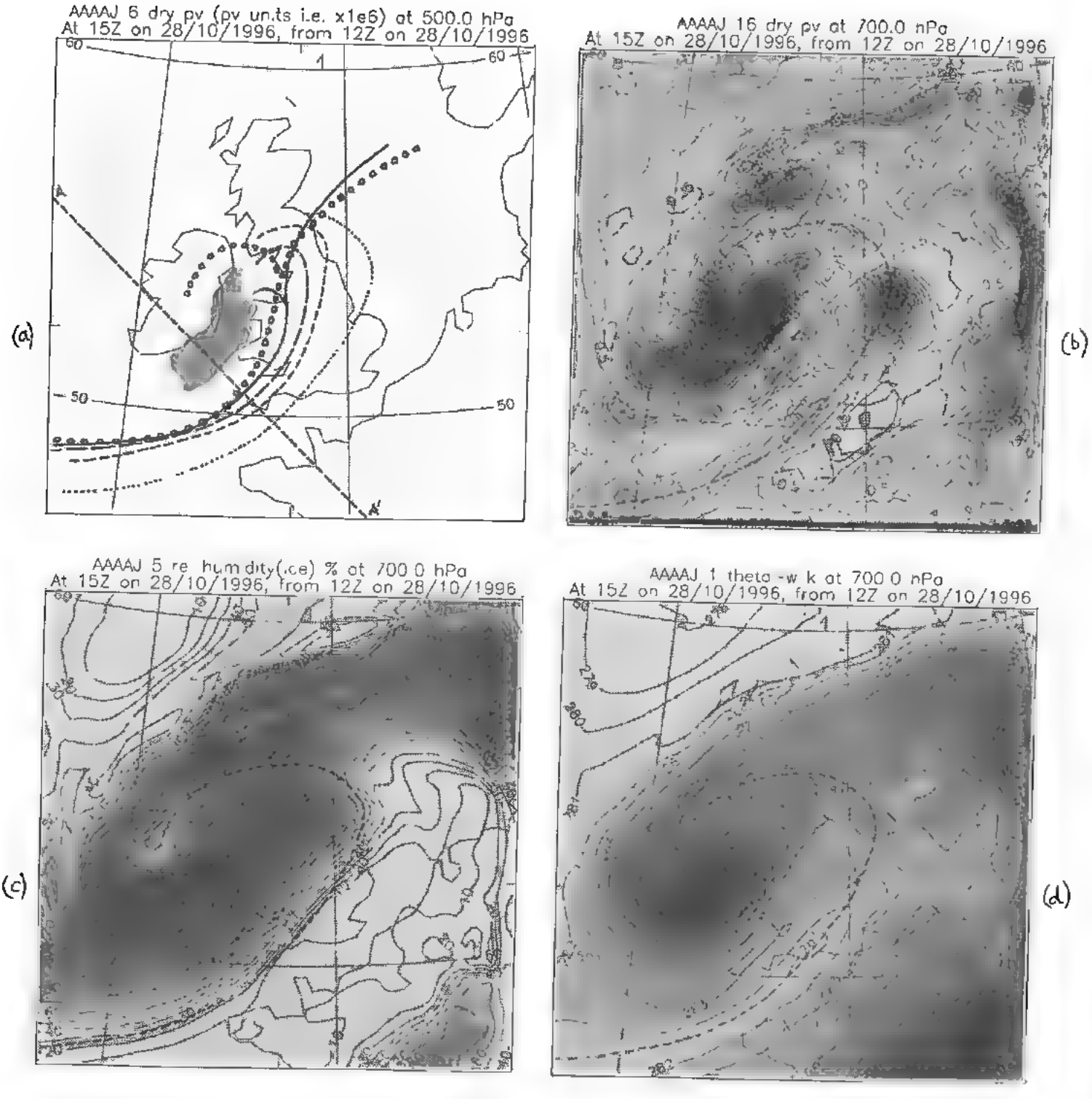
AAAAJ 6 dry pv (pv units i.e. x1e6) at 500.0 hPa
At 15Z on 28/10/1996, from 12Z on 28/10/1996
60
60
50
50
A
A'
(a)
AAAAJ 16 dry pv at 700.0 nPa
At 15Z on 28/10/1996, from 12Z on 28/10/1996
(b)
AAAAJ 5 re humidity(ice) % at 700.0 hPa
At 15Z on 28/10/1996, from 12Z on 28/10/1996
(c)
AAAAJ 1 theta -w k at 700.0 nPa
At 15Z on 28/10/1996, from 12Z on 28/10/1996
(d)

Fig. 15

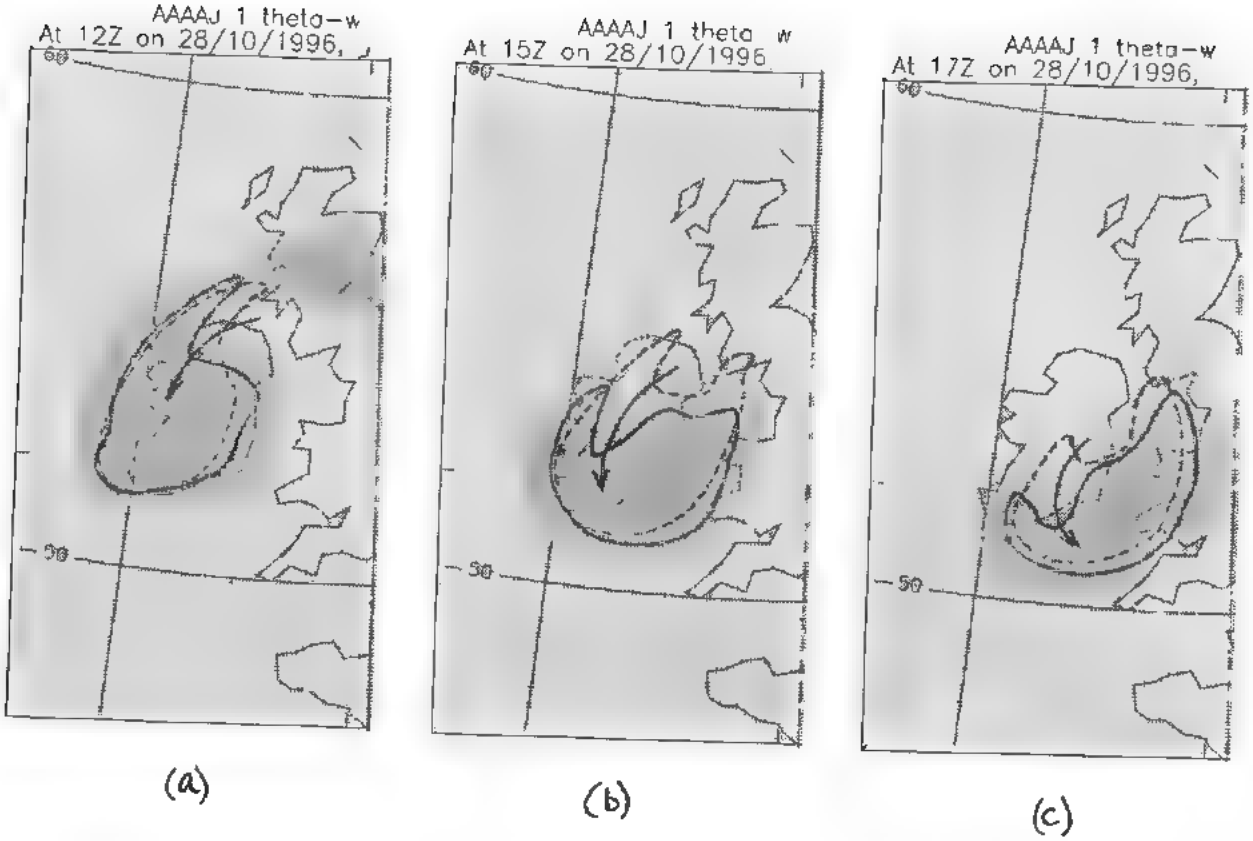
AAAAJ 1 theta-w
At 12Z on 28/10/1996,
60
50
AAAAJ 1 theta w
At 15Z on 28/10/1996
60
50
AAAAJ 1 theta-w
At 17Z on 28/10/1996,
60
50

(a) (b) (c)

Fig 16

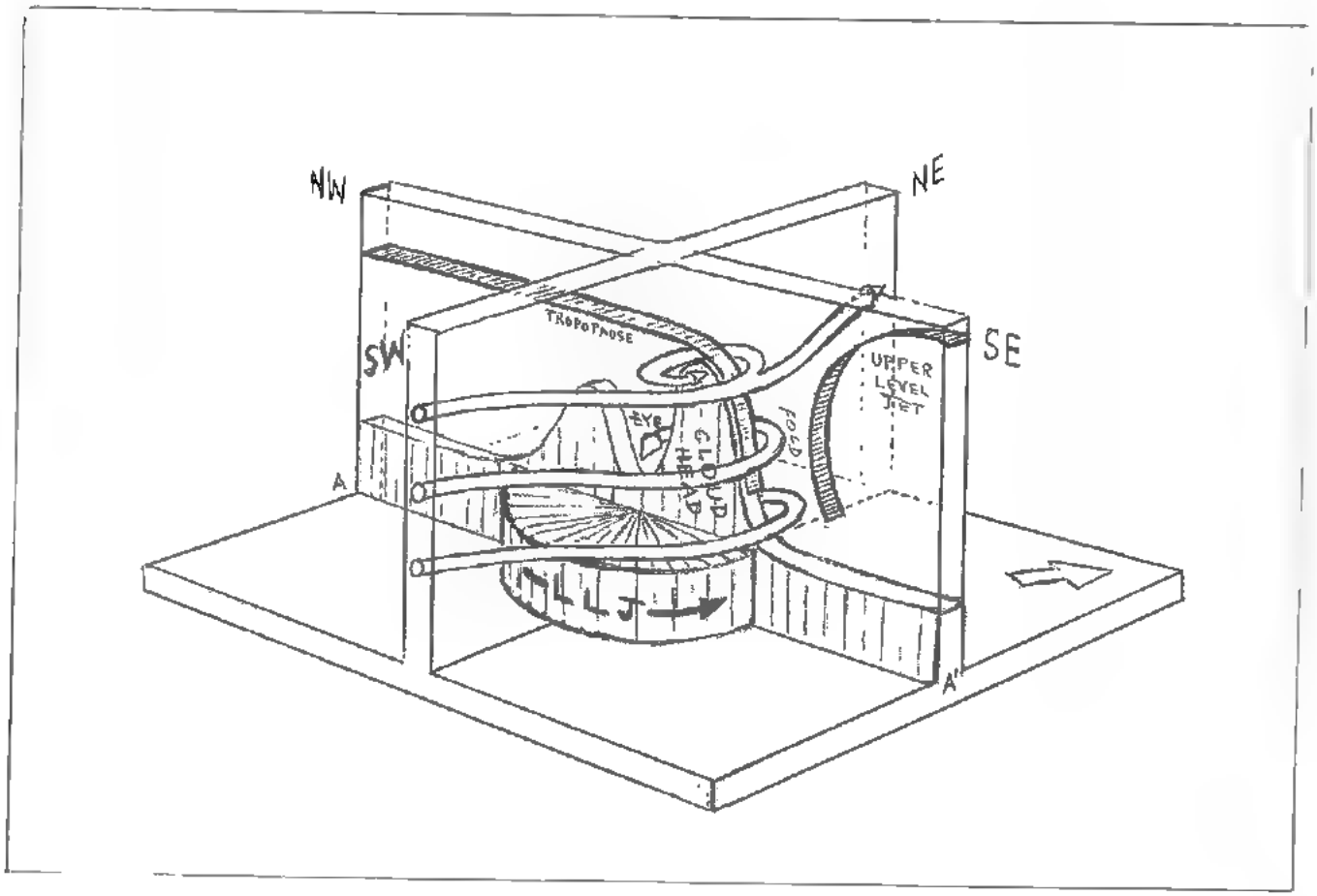
NW
NE
SW
SE
TROPOPAUSE
UPPER LEVEL JET
EYE
COLD AIR
WARM AIR
FOOD
A
A'

Figure 17

CURRENT JCMM INTERNAL REPORTS

This series of JCMM Internal Reports, initiated in 1993, contains unpublished reports and also versions of articles submitted for publication. The complete set of Internal Reports is available from the National Meteorological Library on loan, if required.

1. **Research Strategy and Programme**
   K A Browning et al
   January 1993

2. **The GEWEX Cloud System Study (GCSS)**
   GEWEX Cloud System Science Team
   January 1993

3. **Evolution of a mesoscale upper tropospheric vorticity maximum and comma cloud from a cloud-free two dimensional potential vorticity anomaly**
   K A Browning
   January 1993

4. **The Global Energy and Water Cycle**
   K A Browning
   July 1993

5. **Structure of a midlatitude cyclone before occlusion**
   K A Browning and N Roberts
   July 1993

6. **Development in Systems and Tools for Weather Forecasting**
   K A Browning and G Szejwach
   July 1993

7. **Diagnostic study of a narrow cold frontal rainband and severe winds associated with a stratospheric intrusion**
   K A Browning and R Reynolds
   August 1993

8. **Survey of perceived priority issues in the parametrizations of cloud-related processes in GCMs**
   K A Browning
   September 1993

9. **The Effect of Rain on Longwave Radiation**
   I Dharssi
   September 1993

10. **Physical Cloud Microprocesses - A Description of the Parametrization used in the Large Eddy Model**
    H Swann
    July 1994

11. **An Appreciation of the Meteorological Research of Ernst Kleinschmidt**
A J Thorpe
May 1992

12. **Potential Vorticity of Flow Along the Alps**
A J Thorpe, H Volkert and Dietrich Heimann
August 1992

13. **The Representation of Fronts**
A J Thorpe
January 1993

14. **A Parametrization Scheme for Symmetric Instability: Test for an Idealised Flow**
C S Chan and A J Thorpe
February 1993

15. **The Fronts 92 Experiment: a Quicklook Atlas**
Edited by T D Hewson
November 1993

16. **Frontal wave stability during moist deformation frontogenesis**
Part 1. Linear wave dynamics
C H Bishop and A J Thorpe
May 1993

17. **Frontal wave stability during moist deformation frontogenesis**
Part 2. The suppression of non-linear wave development
C H Bishop and A J Thorpe
May 1993

18. **Gravity waves in sheared ducts**
C Bishop and A J Thorpe
November 1993

19. **Potential Vorticity and the Electrostatics Analogy: Quasi-Geostrophic Theory**
C Bishop and A J Thorpe
November 1993

20. **Recent Advances in the Measurement of Precipitation by Radar**
A J Illingworth
April 1993

21. **Micro-Physique et Givrage. Cloud Microphysics and Aircraft Icing**
A J Illingworth
May 1993

22. **Differential Phase Measurements of Precipitation**
M Blackman and A J Illingworth
May 1993

23. **Estimation of Effective Radius of Cloud Particles from the Radar Reflectivity**
N I Fox and A J Illingworth
May 1993

24. **A Simple Method of Dopplerising a Pulsed Magnetron Radar**
A Hau, A J Illingworth and J Eastment
November 1993

25. **Radiation and Polar Lows**
George C Craig
February 1994

26. **Collected preprints submitted to the International Symposium on the Life Cycles of Extratropical Cyclones; Bergen, Norway, 27 June - 1 July 1994**
April 1994

27. **Convective Frontogenesis**
Douglas J Parker and Alan J Thorpe
April 1994

28. **Improved Measurement of the Ice Water Content in Cirrus Using a Total Water Evaporator**
Philip R A Brown and Peter N Francis
April 1994

29. **Mesoscale Effects of a Dry Intrusion within a Vigorous Cyclone**
K A Browning and B W Golding
April 1994

30. **GEWEX Cloud System Study, Science Plan**
May 1994

31. **Parametrization of Momentum Transport by Convectively Generated Gravity Waves**
R Kershaw
February 1995

32. **Mesoscale Modelling Newsletter No 5**
May 1994

33. **Observations of the mesoscale sub-structure in the cold air of a developing frontal cyclone**
K A Browning, S A Clough, C S A Davitt, N M Roberts and T D Hewson
May 1994

34. **Longwave Radiative Forcing of a Simulated Tropical Squall Line**
Imtiaz Dharssi
July 1994

35. **On the nature of the convective circulation at a kata-cold front**
K A Browning
September 1994

36. **Collective preprints of papers submitted to the COST-75 International Seminar on Advanced Weather Radar Systems, Brussels, 20-23 September 1994**
November 1994

37. **Use of satellite imagery to diagnose events leading to frontal thunderstorms: Parts 1 and 11 of a case study**
K A Browning and N M Roberts
November 1994

38. **The role of spaceborne millimetre-wave radar in the global monitoring of ice cloud**
P R A Brown, A J Illingworth, A J Heymsfield, G M McFarquahar, K A Browning and M Gosset
December 1994

39. **Potential Vorticity Inversion**
Michael Ziemianski
October 1994

40. **Theory of mature tropical cyclones; a comparison between Kleinschmidt (1951) and Emanuel (1986)**
Suzanne L Gray
December 1994

41. **Dispersion and removal of pollutants during the passage of an atmospheric frontal System**
N R Gimson
December 1994

42. **The role of snow sublimation in frontogenesis**
D J Parker and A J Thorpe
December 1994

43. **Potential vorticity and the electrostatics Analogy: Ertel- Rossby formulation**
A J Thorpe and C H Bishop
December 1994

44. **Mesoscale aspect of extratropical cyclones: an observational perspective**
K A Browning
January 1995

45. **A Polar Low Outbreak: Evolution and Mesoscale Structures**
T D Hewson, G C Craig and C Claud
February 1995

46. **Generation of near-surface gusts of deep convection**
K Nakamura and R Kershaw
April 1995

47. **Attribution Concepts applied to the Omega Equation**
S A Clough, C S A Davitt and A J Thorpe
June 1995

48. **Parametrization of mixed-phase cloud and precipitation**
Susan P Ballard and M Gerard Hutchinson
June 1995

49. **Short-range forecasting of stratocumulus: Initialization Prediction**
Susan Ballard, Simon D Jackson and B Macpherson
June 1995

50. **Contributions of the JCMM/Dept of Meteorology Radar Group to the 27th AMS Radar Meteorology Conference, Vail October 1995**
June 1995

51. **Cold Pools in Shear**
Douglas J Parker
September 1995

52. **High-resolution analysis of frontal fracture**
K A Browning, S P Ballard and C S A Davitt
September 1995

53. **The Albedo of Broken Cloud Fields: Calculations using a modified two stream radiation code**
Imtiaz Dharssi and Roy Kershaw
October 1995

54. **Parametrization of momentum transport by convection. I: Theory and cloud modelling results**
P Kershaw and D Gregory
November 1995

55. **Variation of frontal structure along a cold front**
K A Browning and N M Roberts
November 1995

56. **Secondary Frontal Waves**
Douglas Parker
December 1995

57. **Objective Fronts**
T D Hewson
March 1996

58. **Mesoscale analysis of the activation of a cold front during cyclogenesis**
K A Browning, N M Roberts and A J Illingworth
June 1996

59. **Investigation of Different Representations of Rain in a 1-d Evaporation Model**
H Swann
May 1996

60. **Parametrization of diabatic processes in the inversion of the omega-equation**
M Athanassiadou and A J Thorpe

61. **The Role of the Environmental Flow in the Development of Secondary Frontal Cyclones**
I A Renfrew, A J Thorpe and A Joly
June 1996

62. **Consequences of the geostrophic momentum approximation on barotropic instability**
S Malardel, A J Thorpe and A Joly
June 1996

63. **Contributions to the AMS/RMS Conference on Mesoscale Processes**
Reading, 9-13 September 1996

64. **Vorticity and Potential Vorticity in Stratified Flows Interacting with an Isolated Obstacle**
Jorge A Gutierrez and A J Thorpe
September 1996

65. **Triple Point Development: Two Case Studies**
Douglas Parker
September 1996

66. **Radar observations of wind-shear splitting within evolving atmospheric Kelvin-Helmholtz billows**
D Chapman and K A Browning
April 1997

67. **Cold Frontal Structure derived from radar wind profilers**
K A Browning, D Jerrett, J Nash, T Oakley, N M Roberts
May 1997

68. **The dry intrusion and its effect on the frontal, cloud and precipitation structure of extratropical cyclones**
K A Browning - Text of invited special lecture at the Spring Conference of the Meteorological Society of Japan, University of Tsukuba, 22 May 1997

69. **Met. Office Unified Model data, diagnostic graphics programs, and other observational data available from the JCMM through the aegis of the Universities Weather Research Network UWERN.** Plus supplement.
Peter Panagi and Ed Dicks
June 1997

70. **Contributions of the JCMM/Dept of Meteorology Radar Group to 28th AMS Radar Meteorology Conference.** Austin, Texas, September 1997

71. **Sensitivity of short-range weather forecasts to local potential vorticity modifications**
Meral Demirtas and Alan Thorpe
July 1997

72. **Objective identification of frontal wave cyclones**
T D Hewson
August 1997

73. **Attribution and its application to mesoscale structure associated with tropopause folds**
A J Thorpe
September 1997

74. **The Role of the Environmental Flow in the Development of Secondary Frontal Cyclones**
Ian A Renfrew, Alan J Thorpe and Craig H Bishop
September 1997

75. **Potential Vorticity: A short history of its definitions and uses**
Alan J Thorpe and Hans Volkert
September 1997

76. **Superposing Semi-Geostrophic Potential Vorticity Anomalies**
H R Birkett and A J Thorpe
September 1997

77. **Short period forecasting of catchment-scale precipitation. Part 1: the role of Numerical Weather Prediction**
M A Pedder, M Haile and A J Thorpe
September 1997

78. **Verification of the Tracking Technique Used in an Experimental Cloud Motion Wind Inferring System**
Z Wang, K A Browning and G A Kelly
October 1997

79. **A Preliminary Study of Fourier Series Analysis for Cloud Tracking with GOES High Temporal Resolution Images**
Z Wang
October 1997

80. **Analysis of an ex-tropical cyclone after reintensifying as a warm-core extratropical cyclone**
K A Browning, G Vaughan and P Panagi
November 1997

Met Office Joint Centre for Mesoscale Meteorology Department of Meteorology
University of Reading PO Box 243 Reading RG6 6BB United Kingdom
Tel: +44 (0)118 931 8425 Fax: +44 (0)118 931 8791
www.metoffice.com